# Asymptotic fiber orientation states of the quadratically closed Folgar–Tucker equation and a subsequent closure improvement

Tobias Karl, Davide Gatti, Bettina Frohnapfel, and Thomas Böhlke

---

---

# Asymptotic fiber orientation states of the quadratically closed Folgar–Tucker equation and a subsequent closure improvement

Tobias Karl,[1,2,a)] Davide Gatti,[2,b)] Bettina Frohnapfel,[2,c)] and Thomas Böhlke[1,d)]

[1]*Institute of Engineering Mechanics, Chair for Continuum Mechanics, Karlsruhe Institute of Technology (KIT), Karlsruhe, Germany*
[2]*Institute of Fluid Mechanics, Karlsruhe Institute of Technology (KIT), Karlsruhe, Germany*

## Abstract

Anisotropic fiber-reinforced composites are used in lightweight construction, which is of great industrial relevance. During mold filling of fiber suspensions, the microstructural evolution of the local fiber arrangement and orientation distribution is determined by the local velocity gradient. Based on the Folgar–Tucker equation, which describes the evolution of the second-order fiber orientation tensor in terms of the velocity gradient, the present study addresses selected states of deformation rates that can locally occur in complex flow fields. For such homogeneous flows, exact solutions for the asymptotic fiber orientation states are derived and discussed based on the quadratic closure. In contrast to the existing literature, the derived exact solutions take into account the fiber-fiber interaction. The analysis of the asymptotic solutions relying upon the common quadratic closure shows disadvantages with respect to the predicted material symmetry, namely, the anisotropy is overestimated for strong fiber-fiber interaction. This motivates us to suggest a novel normalized fully symmetric quadratic closure. Two versions of this new closure are derived regarding the prediction of anisotropic properties and the fiber orientation evolution. The fiber orientation states determined with the new closure approach show an improved prediction of anisotropy in both effective viscous and elastic composite behaviors. In addition, the symmetrized quadratic closure has a simple structure that reduces the effort in numerical implementation compared to more elaborated closure schemes. © *2021 Author(s). All article content, except where otherwise noted, is licensed under a Creative Commons Attribution (CC BY) license (http://creativecommons.org/licenses/by/4.0/).* https://doi.org/10.1122/8.0000245

## I. INTRODUCTION

### A. Motivation

Composite materials are employed in lightweight designs, thanks to the beneficial properties of their constituents, namely, low mass density, design freedom, high stiffness, and strength [1,2].[1] From the application point of view, fiber-reinforced polymer composites enhance the mechanical properties of conventional materials [1] in order to reduce the mass of components. Short-fiber reinforced polymers manufactured by injection molding are well suited for the manufacturing of mass-produced complex-shaped objects [2]. During mold filling, the complex alignment process of the suspended fibers is determined by the local flow conditions. Flow simulations are carried out for estimating the local fiber orientation state with the goal of predicting the effective anisotropic mechanical properties for composite applications [3]. Employing leading fiber orientation tensors [4,5], closure approximations are required to obtain a solvable system of equations [4,6].

Many different closure methods with varying complexity have been developed [4,6–12]. A compromise is to be found between a structurally simple closure and reliable results to save effort in implementation and computation. Furthermore, the description of the orientation process in fiber suspensions requires suitable modeling of the fiber-fiber interaction mechanism [13]. Even simple fiber-fiber interaction terms in the evolution equation of the fiber orientation state [4,13] complicate the derivation of exact solutions, which are useful for validating numerical computations and for the fundamental understanding of the fiber orientation process [10,11,14,15]. In this context, it is necessary to provide a method covering the effect of the fiber-fiber interaction in terms of exact solutions.

### B. Goals and scope of the study

Within this study, new exact asymptotic solutions for the second-order orientation tensor of the first kind [4,5] based on the Folgar–Tucker equation (FTE) [4,13] are derived and discussed. The fiber-fiber interaction is taken into account. Furthermore, the FTE defining the exact expressions is formulated with the quadratic closure (QC) [4,6,16]. Here, the term "exact" refers only to the analytical expressions regarding the asymptotic solutions obtained for a specific and approximate

---

a)Author to whom correspondence should be addressed; electronic mail: tobias.karl@kit.edu. T.K. contributed to conceptualization, methodology, formal analysis, investigation, data curation, visualization, writing, and reading of the original draft.

b)D.G. contributed to supervision, discussion, writing, review, editing, and reading.

c)B.F. contributed to supervision, funding acquisition, writing, review, editing, and reading.

d)T.B. contributed to conceptualization, discussion, supervision, funding acquisition, writing, review, editing, and reading.

[1]"Preamble of the International Research Training Group GRK 2078 'Integrated engineering of continuous-discontinuous long fiber reinforced polymer structures" (CoDiCoFRP)," https://www.grk2078.kit.edu/index.php (accessed 21 Jan 2021).

closure scheme. The following list summarizes the main content of the present study:

- Exact solutions are provided, which describe the asymptotic fiber orientation state in simple shear flows, elongational flows, planar compression flows and compression flows as a function of the fiber geometry and the fiber-fiber interaction strength. The influence of both parameters is described in detail. Numerical results of a superposed shear and compression flow are also discussed.
- Based on the derived asymptotic solution regarding the simple shear flow, the quality of approximating finite fiber aspect ratios through infinite fiber aspect ratio is formally investigated.
- The aforementioned asymptotic states are compared in terms of the effective anisotropic viscous behavior of the fiber suspension and the elastic properties of the corresponding solid composite, as predicted by the models of Dinh and Armstrong [17] and Mori and Tanaka [18].
- After a detailed analysis of the QC, two versions of an enhanced QC are suggested. The first version improves the reconstruction of orientation data and the estimation of the effective viscous and elastic properties. The second version is formulated in terms of a process-dependent closure function approach to be used in the FTE describing the orientation evolution. In addition, the asymptotic behavior of the FTE based on the common QC is improved by using an adapted fiber-fiber interaction coefficient.

The outline of the paper is as follows. In Sec. I, the problem of the present paper is motivated, the goals and the content of the present study are also described. A brief description of the state of the art concerning exact solutions of fiber orientation states is given, which can be used for validation. Section II contains the description of fibrous microstructures and the governing equation of the present study. In Sec. III, the exact expressions describing the asymptotic orientation states are given with respect to selected deformation rates including symmetric and nonsymmetric velocity gradients. Section IV contains the results and their discussion. In particular, the QC is discussed and improved. The summary and conclusion of the present study are given in Sec. V. A brief discussion of using asymptotic orientation states in the context of reverse engineering is given in the outlook VI. In Appendixes A–I, additional expressions are listed combined with the material parameters in use.

## C. State of the art

In this section, the existing exact solutions of fiber orientation states are reviewed based on the associated description of fibrous microstructures in Sec. II. Please note that the literature review does not consider the fiber-fiber interaction since no exact solutions exist. Furthermore, the exact solutions are limited to isotropic fiber orientation initial states and the following basic assumptions [19–21]:

- The fibers are treated rigid and monodispersely suspended in an incompressible, laminar flow of a Newtonian fluid.
- Inertia, volume forces, and external forces acting on the fibers are not considered.

- The flow is assumed to be spatially homogeneous in a domain, which is much larger than the characteristic length of the fibers.
- The Brownian motion is not considered.

Jeffery and Filon [19] provide ordinary differential equations describing the temporal evolution of two orientation angles for a single fiber immersed in a simple shear flow. In the corresponding exact solution for the angles in three dimensions (3D), two integration constants have to be determined based on the initial fiber orientation state. The same relations are reviewed in Petrie [21]. In Verleye and Dupret [22], Altan *et al.* [23], and in Dinh and Armstrong [17], the exact solution for a single fiber orientation is given as a function of time, depending on the homogeneous time-dependent deformation gradient and on the initial fiber direction in the isotropic orientation state.

The exact solution of the temporal probability density function (PDF) of two orientation angles in a simple shear flow [19,21] is given in Okagawa and Mason [24] and exploited by Moosaie [25] for validation purposes. Altan *et al.* [23] provide the exact solutions for different flow cases restricted to two-dimensional (2D) orientation states. Regarding fiber orientation vectors Kuzmin [10] extends the formulas of Montgomery-Smith *et al.* [11] both for 2D and 3D fiber orientation states. The solution also depends on the temporal deformation gradient of the arbitrary homogeneous flow field.

Exact solutions for the second- and fourth-order fiber orientation tensors of the first kind in 2D are given in Altan and Tang [14]. In the 3D orientation case, Montgomery-Smith *et al.* [11] leverage the exact expression for the PDF to formulate exact integrals for the eigenvalues of the second-order fiber orientation tensor. These integrals are known as the Carlson elliptic integrals [26,27] and can be solved numerically to obtain quasiexact eigenvalue solutions. The integral formulation depends on the eigenvalues of the inverse of the left Cauchy–Green tensor, which can be calculated analytically based on the deformation gradient for the special case of spatially constant velocity gradients [28]. The eigenvectors of the left Cauchy–Green tensor can be used to transform the components of the fiber orientation tensor back to the spatial coordinate system [11].

Ospald [29] provides an exact solution for 2D stationary orientation states based on the FTE closed with QC. This solution can be exploited to validate the spatial development of the fiber orientation in stationary parallel flows. Note that these expressions are limited to infinitely long fibers in order to suppress the periodic reorientation behavior that would be otherwise present in the case of finite fiber lengths with no fiber-fiber interaction. This can be reviewed in the formula of Jeffery's periodic length [11,19,21].

Latz *et al.* [30] study both FTE and an extended FTE with an additional parameter describing the fiber-fiber interaction besides the common Folgar–Tucker term [4,13]. The results present the stationary (asymptotic) values for the fiber alignment in the flow direction as a function of several values of the additional parameter and of the Folgar–Tucker term. Moreover, the results obtained with QC consider only the

case of a simple shear flow with infinitely long fibers and 2D orientation and do not provide exact expressions for the asymptotic state.

Asymptotic behavior of microstructured materials also occurs in other areas of continuum mechanical applications. In Böhlke and Bertram [31], the asymptotic values of the stiffness tensor are discussed for copper subjected to large monotonous deformations. It is shown that such asymptotic values exist for symmetric velocity gradients and depend on the eigenvalues of the strain rate tensor.

## D. Notation

Throughout the present study, a symbolic tensor notation is used. Scalars are denoted by lower case Latin and Greek letters, e.g., $a, b, \alpha, \beta$. Lower case bold letters refer to vectors, e.g., $\mathbf{a}, \mathbf{b}$. Upper case bold letters, e.g., $\mathbf{A}, \mathbf{B}$ represent second-order tensors, whereas upper case blackboard bold letters, e.g., $\mathbb{A}, \mathbb{B}$ denote fourth-order tensors. The scalar product between tensors of equal order is denoted by, e.g., $\mathbf{a} \cdot \mathbf{b}, \mathbf{A} \cdot \mathbf{B}$. The dyadic product between vectors and tensors is indicated by, e.g., $\mathbf{a} \otimes \mathbf{b}, \mathbf{A} \otimes \mathbf{B}$, whereas various compositions and mappings are denoted by, e.g., $\mathbf{Ab}, \mathbf{AB}, \mathbb{A}[\mathbf{B}]$. The material time derivative is represented by a superimposed dot, e.g., $\dot{\mathbf{a}}, \dot{\mathbf{A}}$. The Rayleigh product describes the active rotation of a tensor and is denoted by, e.g., $\mathbf{Q} \star \mathbf{A}, \mathbf{Q} \star \mathbb{A}$ with the orthogonal tensor $\mathbf{Q} \in \text{Orth}^+$. The product $\square$ between two second-order tensors is defined via the mapping $(\mathbf{A} \square \mathbf{C})[\mathbf{B}] = \mathbf{ABC}$. The Frobenius norm of a tensor is denoted by, e.g., $\|\mathbf{A}\| = \sqrt{\mathbf{A} \cdot \mathbf{A}}$ and $\|\mathbf{a}\|_2 = \sqrt{\mathbf{a} \cdot \mathbf{a}}$ refers to the Euclidean vector norm. The trace of a tensor is denoted by, e.g., $\text{tr}(\mathbf{A})$ and the complete symmetry by, e.g., $\text{sym}(\mathbb{A})$. For the dyadic product to generate a tensor of order $n$ the abbreviation $(\cdot)^{\otimes n}$ is used. Please note that the number of operations $\otimes$ depends on the tensor order of the basis $(\cdot)$. When applied to fiber orientation tensors, subscripts, and superscripts refer, respectively, to the tensor order and to the tensor kind. For additional information concerning further tensor operations and for more details, the reader is referred to, e.g., Gurtin *et al.* [28] and Moakher [32]. Note that equations are numbered in blocks rather than lines.

## II. THEORY

### A. Description of fibrous microstructures

The orientation state of a single rigid fiber can be described in spherical coordinates as shown in Fig. 1. The Cartesian base vectors are denoted by $\mathbf{e}_i$ $(i = 1, 2, 3)$. Two orientation angles $\varphi \in [0, 2\pi]$ and $\theta \in [0, \pi]$ are introduced describing all possible orientations on the surface of the unit sphere $\mathscr{S} = \{\mathbf{n} \in \mathscr{R}^3 : \|\mathbf{n}\|_2 = 1\}$ with the fiber direction $\mathbf{n}(\mathbf{x}, t)$ depending on time $t$ and on the actual placement $\mathbf{x}$ as follows [4]:

$$\mathbf{n} = \sin(\theta)\cos(\varphi)\mathbf{e}_1 + \sin(\theta)\sin(\varphi)\mathbf{e}_2 + \cos(\theta)\mathbf{e}_3. \quad (1)$$

The function $f(\mathbf{x}, t, \mathbf{n})$ is called PDF and refers to the probability that a fiber aligns along the direction $\mathbf{n}$ at $(\mathbf{x}, t)$ [4,33].
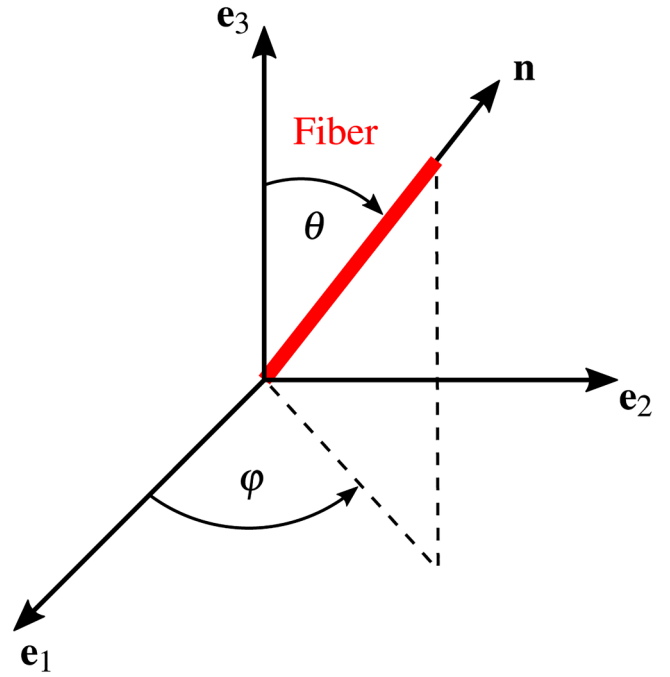


**FIG. 1.** Orientation of a single fiber described in spherical coordinates (own sketch based on Advani and Tucker [4]).

The following mathematical properties hold $\forall \mathbf{x}, t, \mathbf{n}$ [4,33]:

$$f \geq 0, \quad f(\cdot, \mathbf{n}) = f(\cdot, -\mathbf{n}), \quad \int_{\mathscr{S}} f \, \mathrm{d}S = 1, \quad (2)$$

where $\mathrm{d}S = \sin(\theta)\mathrm{d}\theta\mathrm{d}\varphi$ is the surface element on the unit sphere $\mathscr{S}$. Three different kinds of orientation tensors (also called fabric tensors) can be defined according to Kanatani [5] based on the PDF. Tensors of the first kind with arbitrary even order $n$ are denoted by $\mathbb{N}_{\langle n \rangle}^{(1)}(\mathbf{x}, t)$ and defined as follows [4,5]:

$$\mathbb{N}_{\langle n \rangle}^{(1)} = \int_{\mathscr{S}} f \, \mathbf{n}^{\otimes n} \mathrm{d}S. \quad (3)$$

Fiber orientation tensors of the second and third kind are unique and provide information about the anisotropy of the microstructure [5,34]. For conciseness, the definitions of these tensors are provided in Appendix A. Since the orientation tensors of the second and third kind depend on Eq. (3), the expressions given in Sec. III can be used to describe the fibrous microstructure in various ways. The main part of this study is limited to first-kind orientation tensors of second and fourth order denoted as follows for simplicity:

$$\mathbf{N} = \mathbb{N}_{\langle 2 \rangle}^{(1)}, \quad \mathbb{N} = \mathbb{N}_{\langle 4 \rangle}^{(1)}. \quad (4)$$

Please note that the tensors $\mathbf{N}, \mathbb{N}$ are often denoted by $\mathbf{A}, \mathbb{A}$ or $\mathbf{a}_2, \mathbf{a}_4$ or $\langle \mathbf{nn} \rangle, \langle \mathbf{nnnn} \rangle$ in the literature [4,35]. Furthermore, since homogeneous flows are considered in the following, the dependence upon $\mathbf{x}$ in all argument lists above vanishes.

## B. Orientation evolution in fiber suspension flows

In Sec. II A, different methods of describing an existing fibrous microstructure are reviewed. The present section covers the description of the temporal and spatial evolution concerning a microstructured continuum with the assumptions listed in Sec. I C. The modeling is limited to the second- and fourth-order orientation tensors of the first kind $\mathbf{N}$ and $\mathbb{N}$. Furthermore, the fiber-fiber interaction should be considered. In the framework of the present paper and as stated before, the FTE is used as [4,13]

$$\dot{\mathbf{N}} = \mathbf{WN} - \mathbf{NW} + \xi\Big(\mathbf{DN} + \mathbf{ND} - 2\mathbb{N}[\mathbf{D}]\Big) + 2C_{\mathsf{I}}\dot{\gamma}(\mathbf{I} - 3\mathbf{N}). \tag{5}$$

Please note that Eq. (5) differs from the homogenized Jeffery equation [19,36] by the interaction term. In Eq. (5), $\mathbf{D}(\mathbf{x}, t)$ refers to the symmetric part of the velocity gradient $\mathbf{L}(\mathbf{x}, t)$, whereas $\mathbf{W}(\mathbf{x}, t)$ corresponds to the skew-symmetric part. For the special case of incompressible flows $\mathrm{tr}(\mathbf{D}) = 0$ holds. In Eq. (5), $\mathbf{I}$ denotes the second-order identity tensor. The well-known closure problem results from the limitation to leading orientation tensors. In the present paper, $\mathbf{D}$ and $\mathbf{W}$ are assumed to be given. For further information about the coupled problem of fiber suspension flows and the constitutive modeling, the reader is referred to Karl *et al.* [3]. The fiber-fiber interaction strength is described by the isotropic parameter $C_{\mathsf{I}}$ that generally depends on the fiber aspect ratio $\alpha$ and on the fiber volume fraction $\phi$ [37,38]. The shape parameter $\xi$ depends on $\alpha$ and $\dot{\gamma}$ represents the scalar shear rate [4,16]

$$\xi = \frac{\alpha^2 - 1}{\alpha^2 + 1}, \quad \dot{\gamma} = \sqrt{\frac{1}{2}\mathbf{D} \cdot \mathbf{D}} = \frac{\sqrt{2}}{2}\|\mathbf{D}\|. \tag{6}$$

Different expressions of $\dot{\gamma}$ can be obtained if $C_{\mathsf{I}}$ appearing in the exact expressions contained in this work is also corrected accordingly.

It should be noted that the material derivative on the left-hand side of Eq. (5) together with the first two terms on the right-hand side constitute an objective rate of the orientation tensor $\mathbf{N}$, namely, the Jaumann rate. Furthermore, Eq. (5) gives the Jaumann rate of the orientation tensor $\mathbf{N}$ as an isotropic function of $\mathscr{L} = \{\mathbf{D}, \mathbf{N}, \mathbb{N}\}$. The FTE (5) can be rewritten in the following general form with the function of the right-hand side $\mathbf{R}$ and the Jaumann rate on the left-hand side:

$$\dot{\mathbf{N}} - \mathbf{WN} + \mathbf{NW} = \mathbf{R}(\mathscr{L}). \tag{7}$$

The aforementioned isotropic specification follows directly $\forall \mathbf{Q} \in \mathrm{Orth}^+$,

$$\mathbf{Q} \star (\dot{\mathbf{N}} - \mathbf{WN} + \mathbf{NW}) = \mathbf{R}(\mathbf{Q} \star \mathscr{L}), \tag{8}$$

which means that actively rotated input arguments $\mathscr{L}$ result in an active rotation of the Jaumann rate of $\mathbf{N}$.

## III. ASYMPTOTIC FIBER ORIENTATION STATES

### A. General implicit formulation

In the following, a general approach for determining the asymptotic states of the FTE is presented. Please note that the formulas in this section are not limited to a specific closure. Therefore, the fourth-order orientation tensor $\mathbb{N}$ is treated to be given by a general closure function $\mathbb{F}(\mathbf{N})$ leading to the asymptotic FTE

$$\mathbf{0} = \mathbf{WN} - \mathbf{NW} + \xi\Big(\mathbf{DN} + \mathbf{ND} - 2\mathbb{F}(\mathbf{N})[\mathbf{D}]\Big) + 2C_{\mathsf{I}}\dot{\gamma}(\mathbf{I} - 3\mathbf{N}). \tag{9}$$

The asymptotic solutions of the commonly used reduced-strain closure model [39] coincide with those of the FTE [40]. An asymptotic solution is an orientation state that for a fixed observer and given velocity gradient is independent of time for a specific material point. Furthermore, the actual rate of deformation does not affect the asymptotic solution, which makes it possible to simplify the governing equations for given flow kinematics (see Appendixes C–G). Equation (9) can be reformulated compactly as follows representing an implicit equation for the asymptotic state $\mathbf{N}$:

$$\mathbf{0} = \mathbb{K}[\mathbf{N}] - 2\xi\mathbb{F}(\mathbf{N})[\mathbf{D}] + 2C_{\mathsf{I}}\dot{\gamma}\mathbf{I}, \tag{10}$$

where the fourth-order tensor $\mathbb{K}$ describing the main part of the given kinematic state is defined by

$$\mathbb{K} = (\mathbf{W}\square\mathbf{I})^{\mathsf{S}} - (\mathbf{I}\square\mathbf{W})^{\mathsf{S}} + \xi(\mathbf{D}\square\mathbf{I})^{\mathsf{S}} + \xi(\mathbf{I}\square\mathbf{D})^{\mathsf{S}} - 6C_{\mathsf{I}}\dot{\gamma}\mathbb{I}^{\mathsf{S}}. \tag{11}$$

The operator $(\cdot)^{\mathsf{S}}$ and the identity on symmetric second-order tensors $\mathbb{I}^{\mathsf{S}}$ are defined by

$$(\mathbf{A}\square\mathbf{B})^{\mathsf{S}} = \frac{1}{2}\big(\mathbf{A}\square\mathbf{B} + (\mathbf{A}\square\mathbf{B})^{\mathsf{T_R}}\big), \quad \mathbb{I}^{\mathsf{S}} = (\mathbf{I}\square\mathbf{I})^{\mathsf{S}}. \tag{12}$$

It is pointed out that $\mathbb{K}$ is anisotropic since $\mathbb{K} \neq \mathbf{Q} \star \mathbb{K}$ holds $\forall \mathbf{Q} \in \mathrm{Orth}^+$. In contrast, $\mathbb{K}$ is an isotropic function of its arguments $\mathbf{D}$ and $\mathbf{W}$. Based on general flows the kinematic tensor $\mathbb{K}$ has both minor symmetries but no main symmetry

$$\mathbb{K} \neq \mathbb{K}^{\mathsf{T_H}} \Leftrightarrow K_{ijkl} \neq K_{klij},$$
$$\mathbb{K} = \mathbb{K}^{\mathsf{T_R}} \Leftrightarrow K_{ijkl} = K_{ijlk}, \tag{13}$$
$$\mathbb{K} = \mathbb{K}^{\mathsf{T_L}} \Leftrightarrow K_{ijkl} = K_{jikl}.$$

Note that for spin-free flows $\mathbb{K} = \mathbb{K}^{\mathsf{T_H}} = \mathbb{K}^{\mathsf{T_R}} = \mathbb{K}^{\mathsf{T_L}}$ is valid. In the case of pure spin $\mathbb{K} = -\mathbb{K}^{\mathsf{T_H}} = \mathbb{K}^{\mathsf{T_R}} = \mathbb{K}^{\mathsf{T_L}}$ holds with the vanishing trace $\mathrm{tr}(\mathbb{K}) = \mathbb{K} \cdot \mathbb{I} = 0$. Note that the identity tensor $\mathbb{I}$ is defined by $\mathbb{I} = \mathbf{I}\square\mathbf{I}$. In the following, the QC $\mathbb{F}(\mathbf{N}) = \mathbb{N}_{\mathsf{QC}} = \mathbf{N} \otimes \mathbf{N}$ is used combined with simple flow kinematics leading to exact solutions for $\mathbf{N}$ based

on Eq. (10). One example of a superposed flow illustrates that even simple flows require numerical solution procedures.

## B. Spin-free flows

Before the spin-free (irrotational) flows under consideration are specified more precisely, a formal definition should be made. In case of incompressibility, the definition of spin-free flows turns out to be a one-dimensional problem by setting the parameter $\Lambda \in [-0.5, 0.5]$ appropriately as [41]

$$\mathbf{D} = \|\mathbf{D}\|\mathbf{Q}_D\mathbf{D}_0\mathbf{Q}_D^\mathsf{T}, \quad \mathbf{D}_0 = \sum_{i=1}^{3} D_i \mathbf{e}_i^\mathsf{H} \otimes \mathbf{e}_i^\mathsf{H},$$

$$D_{1,3} = -\frac{\sqrt{6}}{6}\Lambda \pm \frac{\sqrt{2}}{2}\sqrt{1-\Lambda^2}, D_2 = \frac{\sqrt{6}}{3}\Lambda. \tag{14}$$

In Eq. (14), the tensor $\mathbf{Q}_D \in \mathrm{Orth}^+$ defines a mapping between $\{\mathbf{e}_i\}$ and the eigensystem $\{\mathbf{e}_i^\mathsf{H}\}$ of $\mathbf{D}$ ($i = 1, 2, 3$) [41]. The eigenvalues of the direction $\mathbf{D}_0 = \mathbf{D}/\|\mathbf{D}\|$ are represented by $D_i$ ($i = 1, 2, 3$) [41]. In the following, the spin-free flows under consideration are described with an arbitrary scalar quantity $a > 0\,\mathrm{s}^{-1}$ representing the rate of deformation.

### 1. Elongational flow ($\Lambda = -0.5$)

The kinematics of an elongational flow in direction $\mathbf{e}_1$ (see Fig. 2, also known as uniaxial elongation) is described as follows with $\mathbf{W} = \mathbf{0}\,\mathrm{s}^{-1}$ and

$$\mathbf{D} = a\mathbf{e}_1 \otimes \mathbf{e}_1 - \frac{a}{2}(\mathbf{e}_2 \otimes \mathbf{e}_2 + \mathbf{e}_3 \otimes \mathbf{e}_3). \tag{15}$$

The asymptotic state of $\mathbf{N}$ based on the governing system of equations described in Appendix C is as follows with the parameter $\psi$ depending on $\xi$ and $C_1$ according to Eq. (C3),

$$N_{11} = \psi, \quad N_{22} = N_{33} = \frac{\sqrt{3}C_1\psi}{3\xi\psi + \sqrt{3}C_1},$$

$$N_{12} = N_{13} = N_{23} = 0. \tag{16}$$

### 2. Planar compression flow ($\Lambda = 0.0$)

The kinematics of a planar compression flow in the $\mathbf{e}_1$–$\mathbf{e}_3$-plane (see Fig. 2, also known as planar elongation) is

described as follows with $\mathbf{W} = \mathbf{0}\,\mathrm{s}^{-1}$ and

$$\mathbf{D} = a(\mathbf{e}_1 \otimes \mathbf{e}_1 - \mathbf{e}_3 \otimes \mathbf{e}_3). \tag{17}$$

The asymptotic state of $\mathbf{N}$ based on the governing system of equations described in Appendix D is as follows with the parameter $\psi$ depending on $\xi$ and $C_1$ according to Eq. (D3),

$$N_{11} = \psi, \quad N_{33} = \frac{1}{\xi\psi}\left(\xi\psi^2 + (3C_1 - \xi)\psi - C_1\right),$$

$$N_{22} = 1 - N_{11} - N_{33}, \quad N_{12} = N_{13} = N_{23} = 0. \tag{18}$$

### 3. Compression flow ($\Lambda = 0.5$)

The kinematics of a compression flow in direction $-\mathbf{e}_3$ (see Fig. 2, also known as biaxial elongation) is described as follows with $\mathbf{W} = \mathbf{0}\,\mathrm{s}^{-1}$ and

$$\mathbf{D} = \frac{a}{2}(\mathbf{e}_1 \otimes \mathbf{e}_1 + \mathbf{e}_2 \otimes \mathbf{e}_2) - a\mathbf{e}_3 \otimes \mathbf{e}_3. \tag{19}$$

The asymptotic state of $\mathbf{N}$ based on the governing system of equations described in Appendix E is as follows with the parameter $\psi$ depending on $\xi$ and $C_1$ according to Eq. (E3),

$$N_{11} = N_{22} = \frac{\sqrt{3}C_1\psi}{\sqrt{3}C_1 - 3\xi\psi}, \quad N_{33} = \psi,$$

$$N_{12} = N_{13} = N_{23} = 0. \tag{20}$$

Note that both the material derivative and the Jaumann rate of $\mathbf{N}$ vanish in case of the asymptotic state in spin-free deformation processes. The resulting system of equations does not depend on the magnitude $\|\mathbf{D}\|$ but on the directional information $\mathbf{D}/\|\mathbf{D}\|$. This is discussed in the context of Fig. 10. Since the orientation state is assumed to be isotropic at the beginning, $\mathbf{Q}_D = \mathbf{I}$ holds [41].

## C. Simple shear flow

The kinematics of a simple shear flow in $\mathbf{e}_1$ (see Fig. 2) is described by the following tensors $\mathbf{D}$ and $\mathbf{W}$ with an arbitrary scalar quantity $a > 0\,\mathrm{s}^{-1}$:

$$\mathbf{D} = a(\mathbf{e}_1 \otimes \mathbf{e}_2 + \mathbf{e}_2 \otimes \mathbf{e}_1), \quad \mathbf{W} = a(\mathbf{e}_1 \otimes \mathbf{e}_2 - \mathbf{e}_2 \otimes \mathbf{e}_1). \tag{21}$$

The asymptotic state $\mathbf{N}$ based on the governing system of equations described in Appendix F is as follows with the
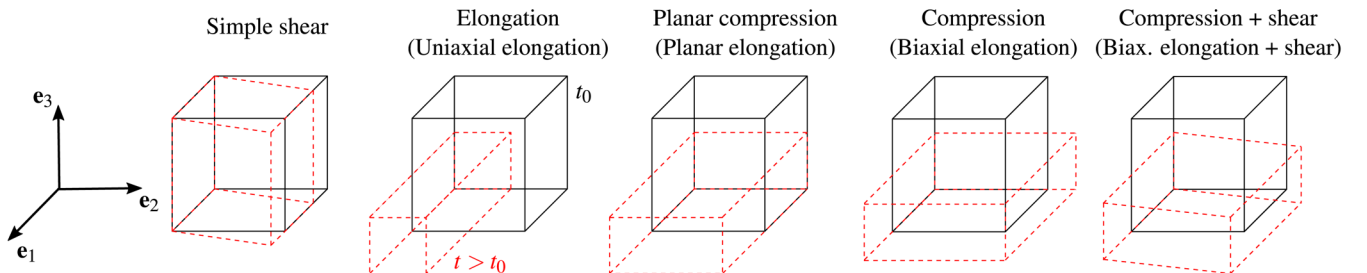


**FIG. 2.** Visualization of the investigated flow cases via incompressible fluid particle deformations with respect to the given spatial coordinate system (solid: reference placement $t = t_0$, dashed: actual placement $t > t_0$).

parameter $\psi$ depending on $\xi$ and $C_I$ according to Eq. (F3),

$$
\begin{aligned}
N_{11} &= \frac{(\xi+1)\psi + C_I}{2\xi\psi + 3C_I}, \quad N_{22} = \frac{(\xi-1)\psi + C_I}{2\xi\psi + 3C_I}, \\
N_{33} &= \frac{C_I}{2\xi\psi + 3C_I}, \quad N_{12} = \psi, \\
N_{13} &= 0, \quad\quad\quad\quad\quad N_{23} = 0.
\end{aligned} \tag{22}
$$

As stated before that the shape parameter $\xi$ is a function of the fiber aspect ratio $\alpha$. Please note that in the framework of the present paper $C_I = 0$ in combination with $1 < \alpha < \infty$ is not allowed since there is periodic reorientation arising for this parameter set. Furthermore, using the FTE for considering the fiber-fiber interaction only makes sense for $C_I > 0$.

## D. Compression flow superposed with simple shear

The kinematics of a compression flow in the direction $-\mathbf{e}_3$ superposed with a simple shear flow in the direction $\mathbf{e}_1$ (see Fig. 2, also known as biaxial elongation superposed with shear) is described by the following tensors $\mathbf{D}$ and $\mathbf{W}$ with the arbitrary scalar quantities $a, b > 0\,\mathrm{s}^{-1}$:

$$
\mathbf{D} = \frac{a}{2}(\mathbf{e}_1 \otimes \mathbf{e}_1 + \mathbf{e}_2 \otimes \mathbf{e}_2) - a\mathbf{e}_3 \otimes \mathbf{e}_3 + b(\mathbf{e}_1 \otimes \mathbf{e}_2 + \mathbf{e}_2 \otimes \mathbf{e}_1),
$$

$$
\mathbf{W} = b(\mathbf{e}_1 \otimes \mathbf{e}_2 - \mathbf{e}_2 \otimes \mathbf{e}_1). \tag{23}
$$

This flow can be seen as an example of a superposition consisting of already discussed flows. The quantity $a$ represents the compression rate, whereas $b$ refers to the shear rate. Besides the directional information within the sign of $a, b$, the ratio $a/b$ turns out to influence the asymptotic state

$$
\frac{a}{b} = \frac{\text{Compression rate}}{\text{Shear rate}}. \tag{24}
$$

Although the kinematic state is simple, it is not possible to provide exact expressions for the asymptotic orientation state. The governing system of equations given in Appendix G for arbitrary $a, b$ is, therefore, solved numerically for different parameters $\xi$ and $C_I$. In the framework of the present paper, three different ratios $a/b > 0$ are considered.

## IV. RESULTS AND DISCUSSION

## A. Fiber orientation tensor components

In Fig. 3, the asymptotic fiber orientation states are shown for the spin-free flows as a function of the fiber aspect ratio $\alpha$ and the interaction parameter $C_I$. In Fig. 4, the shear flow and the numerical results of the compression flow superposed with a simple shear flow are shown. The nonzero components $N_{ij}$ are sorted by column and the flow cases by line, respectively. Since $N_{12} = 0$ for spin-free flows, the eigensystem of $\mathbf{N}$ is equal to the spatial coordinate system. It is recalled that the fiber aspect ratio $\alpha$ and the form parameter $\xi$ both describe the geometry of the fibers as given in Eq. (6). The considered ranges $\alpha \in [2, 100]$ and $C_I \in [10^{-4}, 1]$ are

chosen arbitrarily keeping in mind that $C_I > 0.1$ is only used to showcase the effect of $C_I$ but is typically not encountered in applications. As already addressed in Sec. II B, $C_I$ is not an independent parameter. Regarding Fig. 3 and the shear flow in Fig. 4 which are based on exact expressions, the results of the special cases follow directly from the given equations for $\psi$ and $N_{ij}$. The phenomenological behavior of the numerical solutions in Fig. 4 can be interpreted in light of the exact expressions. In the following, the asymptotic orientation states are discussed based on special cases of the parameters $\alpha$ and $C_I$:

- $C_I \to 0$ and $1 < \alpha < \infty$ ($0 < \xi \le 1$): This special case is characterized by a vanishing fiber-fiber interaction. By looking at Eq. (5), the FTE represents the counterplay between the spin terms and the strain rate terms weighted by $\xi$. For finitely long fibers $\xi < 1$ leads to a dominating spin, which results in a periodic orientation behavior already known from the literature [11,14] and commonly referred to as a Jeffery orbit. Since only asymptotic orientation states should be considered throughout this work, $\alpha \to \infty$ ($\xi = 1$) only is allowed which leads to a perfect alignment related to the given kinematics. For the compression flow the planar isotropic (PI) state is the preferred one and the unidirectional state (UD) for all other investigated flows, respectively.

- $C_I \to \infty$ and $1 < \alpha < \infty$ ($0 < \xi \le 1$): This special case is characterized by a dominating fiber-fiber interaction term

$$
2C_I \dot{\gamma}(\mathbf{I} - 3\mathbf{N}) = 6C_I \dot{\gamma}(\mathbf{N}_{\mathsf{ISO}} - \mathbf{N}), \tag{25}
$$

which represents a driving force toward the isotropic orientation state (ISO) [40]. This effect can be seen for all investigated flow cases albeit to a different extent in relation to the selected parameters.

- $C_I \ge 0$ and $\alpha \to 1$ ($\xi \to 0$): This special case is characterized by suspended particles with spherical geometry. By definition, the corresponding tensor $\mathbf{N}$ is isotropic meaning that only a uniform fiber orientation distribution can be identified. Based on the FTE (9) or (10) for $\xi \to 0$, no directional influence of $\mathbf{D}$ is present. Since $\mathbf{N}$ is assumed to be isotropic at the beginning, also nonvanishing tensors $\mathbf{W}$ do not influence the evolution of $\mathbf{N}$. The interaction term depending on the scalar representation $\dot{\gamma}$ of $\mathbf{D}$ equals zero, since $\mathbf{N}$ stays isotropic. Therefore, anisotropic material symmetries cannot be generated by suspended spherical particles. In other words, statistical isotropy follows directly if the microstructure is assumed to be statistically homogeneous [42].

- $C_I \ge 0$ and $\alpha \to \infty$ ($\xi \to 1$): For the case $C_I = 0$ the reader is referred to the first special case discussed in this section. Furthermore and as described before, increasing values of $C_I$ force the fiber orientation toward the isotropic state.

In the context of the latter special case discussed above, the following question arises: In which range is $\alpha \to \infty$ a feasible simplification, even if $\alpha$ is finite? For fixed $C_I$ the value of $\alpha$ influences the FTE via the shape parameter $\xi$
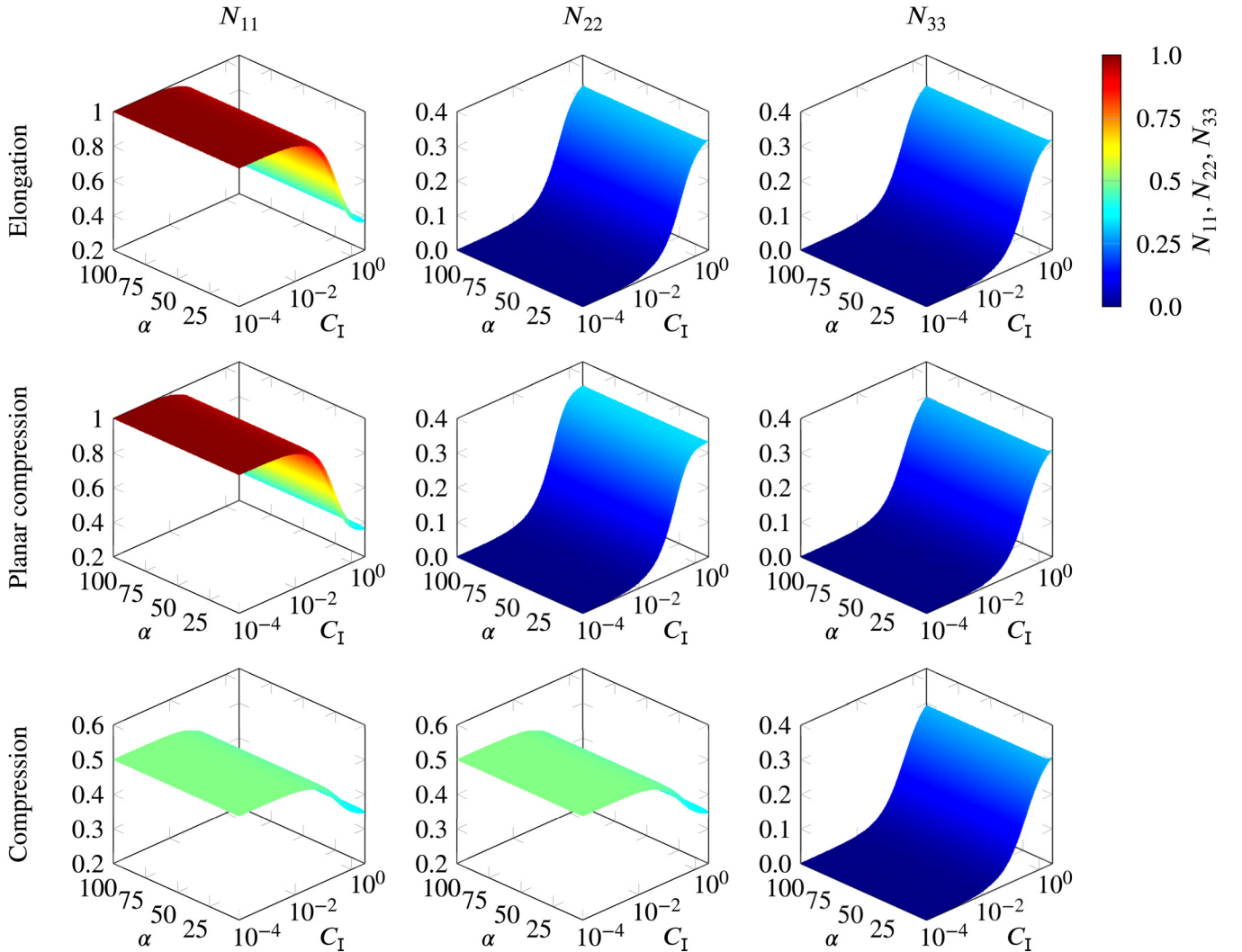
**FIG. 3.** Asymptotic fiber orientation tensor components $N_{ij}$ (columns) for the spin-free flows (rows) with respect to the parameters $\alpha$ and $C_I$ (orientation states given analytically, QC).

given in Eq. (6). By investigating $|\xi(\alpha \to \infty) - \xi(\alpha)|$ shown in Fig. 5, one can see that the latter difference between $\xi = 1$ ($\alpha \to \infty$) and $\xi$ for finite $\alpha$ decreases rapidly. In addition, the simplification $\alpha \to \infty$ for finite $\alpha$ is investigated based on the difference of the asymptotic solutions $|N_{ij}(\alpha \to \infty) - N_{ij}(\alpha)|$ shown in the top plots of Fig. 6. The bottom plots show the behavior of the asymptotic solution $N_{ij}(\alpha)$ itself. The plots are limited to the simple shear flow commonly present in injection molding and to four different values of $C_I$. The results of the top plots show the decrease of the difference between the asymptotic solution based on $\alpha \to \infty$ and on finite $\alpha$. According to Brylka [43] any $\alpha > 100$ delivers practically identical results compared to $\alpha \to \infty$ in the context of the Mori–Tanaka (MT) homogenization method given in Eq. (27) for UD and PI orientation states. Therefore, instead of using finite $\alpha > 100$, the simplification $\alpha \to \infty$ is sufficient and hardly affects the results. Please note that the different behavior shown in the top plots of Fig. 6 is directly linked to the plots below. Furthermore, the larger $C_I$ the faster the plotted difference decreases with increasing $\alpha$. This is based on the fact that growing $C_I$

dominates the FTE by forcing the solution to be isotropic, independent of $\alpha$. In addition, the investigation of $\xi$ and the asymptotic solutions $N_{ij}(\alpha)$ justifying the simplification $\alpha \to \infty$ does not limit the generality, since the sensitivity of the FTE on $\alpha$ for a fixed $C_I$ is completely covered.

## B. Effective viscous and elastic anisotropy

The anisotropic viscous and elastic behavior is studied for the asymptotic orientation states and the flow conditions discussed in Sec. III. The effective viscosity is linked to fiber suspensions with flow-dependent anisotropic orientation states, whereas the effective elasticity refers to the suspension after its fluid-solid transition. On the one hand, the viscosity is an important quantity affecting the flow of the fiber suspension in a coupled sense [3]. On the other hand, the effective stiffness allows conclusions to be drawn in the sense of dimensioning after the fluid-solid transition during processing [3].

To evaluate the effect of the fiber induced viscous behavior the model of Dinh and Armstrong [17] is used in terms of the dimensionless viscosity tensor $\mathbb{V}^* = \mathbb{V}/\eta_M$ normalized
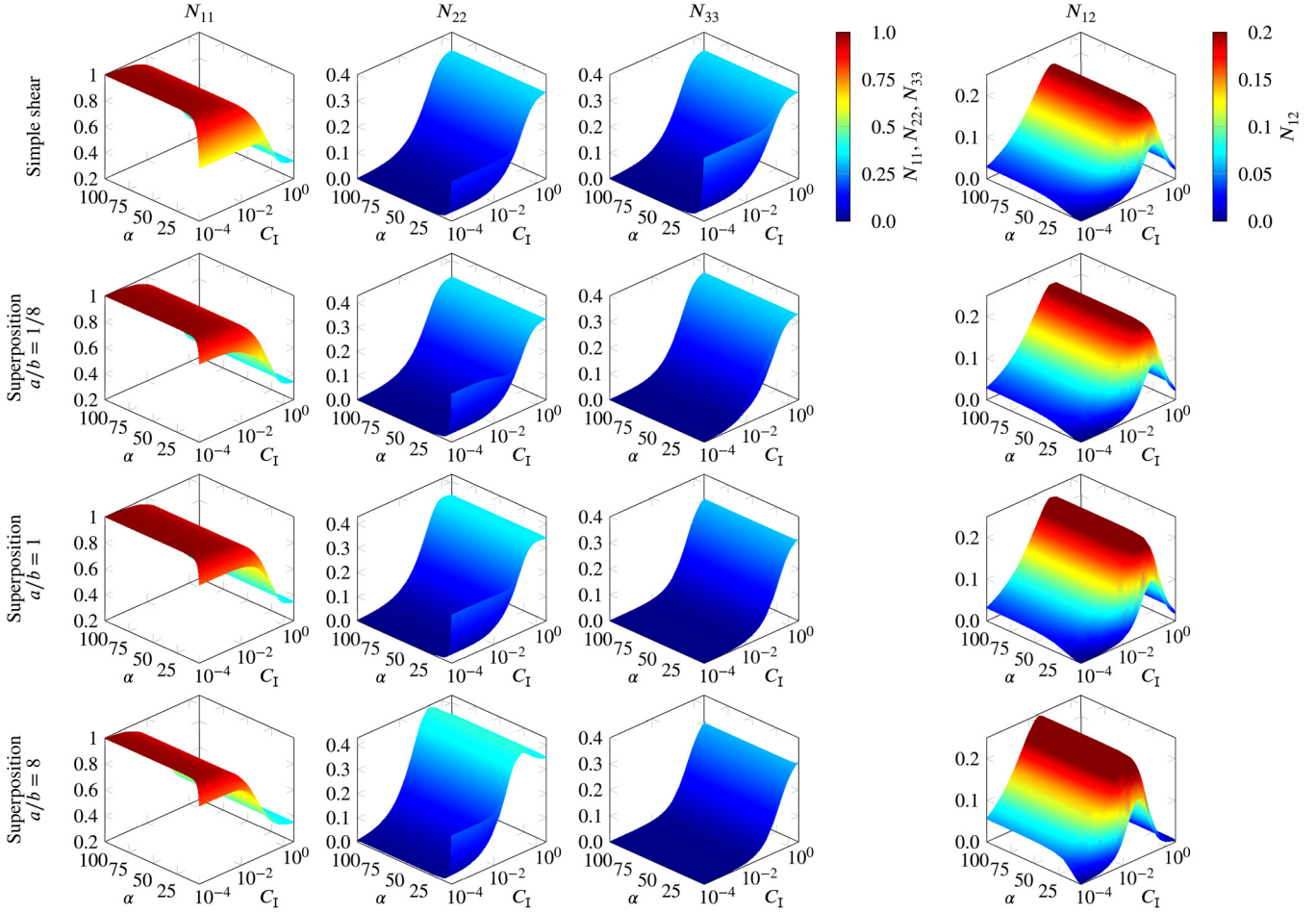
**FIG. 4.** Asymptotic fiber orientation tensor components $N_{ij}$ (columns) for the simple shear and for the superposed flow for different magnitude ratios $a/b$ (rows) with respect to the parameters $\alpha$ and $C_I$ ($a$: compression rate, $b$: shear rate, simple shear given analytically, superposed flow solved numerically, QC).

with the homogeneous matrix shear viscosity $\eta_M$ [3,35,44]

$$\mathbb{V}^* = 2\mathbb{P}_2 + \eta_1^* \mathbb{N}, \quad \eta_1^* = \frac{2\phi\alpha^2}{3\ln(\sqrt{\pi/\phi})}. \tag{26}$$
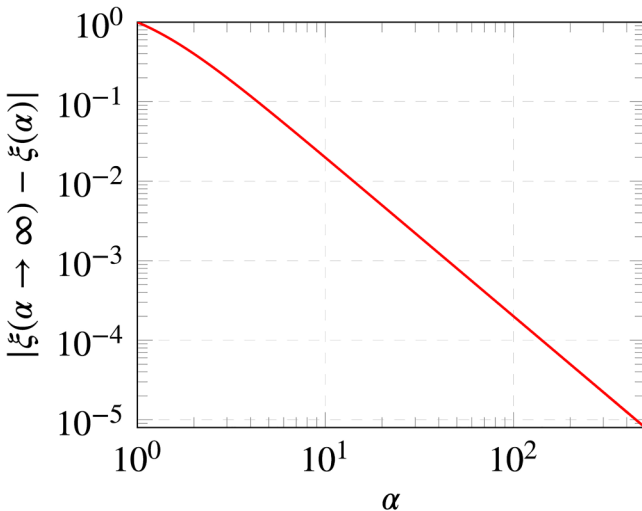


**FIG. 5.** Absolute value of the difference in the shape parameter $\xi(\alpha)$ regarding infinite and finite aspect ratios $\alpha$.

In Eq. (26), $\mathbb{P}_2$ represents the projector on the symmetric traceless tensors with $\mathbb{P}_2 = \mathbb{I}^S - \mathbb{P}_1$, $\mathbb{I}^S$ defined in Eq. (12) and the projector on spherical tensors $\mathbb{P}_1 = \mathbf{I} \otimes \mathbf{I}/3$. The fiber volume fraction is described by $\phi$ and the dimensionless additional shear viscosity is denoted by $\eta_1^* = \eta_1/\eta_M$. Please note that only incompressible flows are considered.

The anisotropic stiffness tensor $\bar{\mathbb{C}}^{MT}$ of the solid composite based on a known fiber orientation state is determined using the MT method [3,18,43]

$$\bar{\mathbb{C}}^{MT} = \mathbb{C}_M + \phi \left[ (1 - \phi)\langle \mathbb{T} \rangle_{OA}^{-1} + \phi(\mathbb{C}_F - \mathbb{C}_M)^{-1} \right]^{-1},$$
$$\mathbb{T} = \left( \mathbb{P}_0 + (\mathbb{C}_F - \mathbb{C}_M)^{-1} \right)^{-1}. \tag{27}$$

In Eq. (27), $\mathbb{C}$ stands for the stiffness tensor and the indices M and F denote the matrix and the fiber material, respectively. The polarization tensor $\mathbb{P}_0$ depends on the matrix stiffness and on the shape of the inclusions, which are assumed to be ellipsoidal with a circular cross section. The operation $\langle \cdot \rangle_{OA}$ refers to the orientation average (OA) scheme applied to $\mathbb{T}$ taking into account the fiber orientation $\mathbf{N}$ and $\mathbb{N}$ [4]
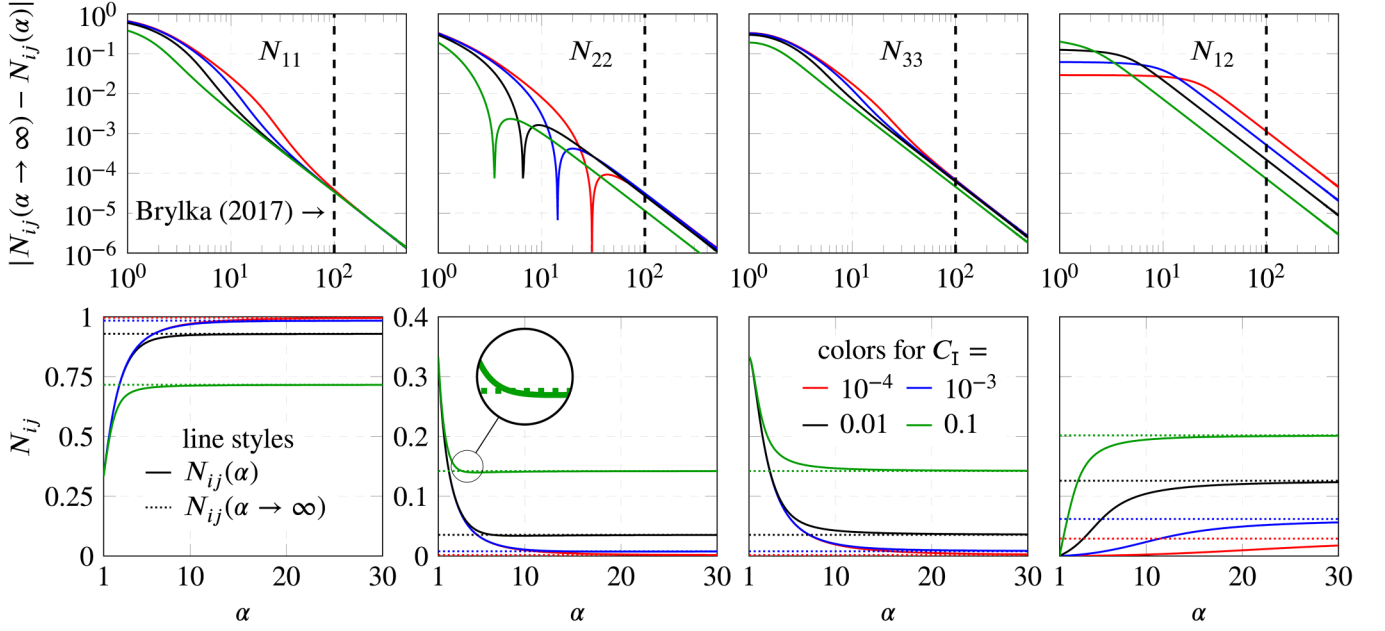
**FIG. 6.** Absolute value of the difference in the asymptotic shear flow solution $N_{ij}$ regarding infinite and finite aspect ratios $\alpha$ (top plots) and the asymptotic shear flow solution $N_{ij}$ plotted against $\alpha$ (bottom plots) for the QC.

$$\langle \mathbb{T} \rangle_{\mathsf{OA}} = b_1 \mathbb{N} + b_2 (\mathbf{N} \otimes \mathbf{I} + \mathbf{I} \otimes \mathbf{N})$$
$$+ b_3 (\mathbf{N} \square \mathbf{I} + (\mathbf{N} \square \mathbf{I})^{\mathsf{T_R}} + \mathbf{I} \square \mathbf{N} + (\mathbf{I} \square \mathbf{N})^{\mathsf{T_R}})$$
$$+ b_4 \mathbf{I} \otimes \mathbf{I} + b_5 \mathbb{I}^{\mathsf{S}}. \tag{28}$$

The coefficients $b_i$ ($i = 1, \ldots, 5$) depend on the given tensor $\mathbb{T}$ as follows [4,45]:

$$b_1 = T_{1111} + T_{2222} - 2T_{1122} - 4T_{1212},$$
$$b_2 = T_{1122} - T_{2233},$$
$$b_3 = T_{1212} + (T_{2233} - T_{2222})/2, \tag{29}$$
$$b_4 = T_{2233},$$
$$b_5 = T_{2222} - T_{2233}.$$

Further information about the assumptions and the properties of the tensors involved can be found in Karl *et al.* [3] and the literature therein and are not reported here for conciseness. The main assumption is that both the fiber and the matrix material are isotropic and linear elastic. Also, the effective behavior of the composite is assumed to be linear elastic.

The anisotropy of the viscous and the elastic behavior is represented by the scalar viscosity $\eta^*(\varphi)$ and by Young's modulus $\bar{E}(\varphi)$ in the $\mathbf{e}_1$–$\mathbf{e}_2$-plane ($\theta = \pi/2$) as shown in Fig. 7. In the case of stiffness investigations, $\mathbf{d}$ refers to the tensile direction [Fig. 7(a)], whereas $\mathbf{d}$ stands for the shear direction is case of viscosity investigations [Fig. 7(b)]. In the related equations, the normalized Voigt notation [46,47] is used with respect to the fourth-order tensors. The following expressions are used to determine $\eta^*$ and $\bar{E}$ [46]:

$$\eta^* = \left( 2\sqrt{2}\,\text{sym}(\mathbf{p} \otimes \mathbf{d}) \cdot \mathbb{V}^{*-1}[\sqrt{2}\,\text{sym}(\mathbf{p} \otimes \mathbf{d})] \right)^{-1},$$
$$\bar{E} = \left( \mathbf{d} \otimes \mathbf{d} \cdot (\bar{\mathbb{C}}^{\mathsf{MT}})^{-1}[\mathbf{d} \otimes \mathbf{d}] \right)^{-1}. \tag{30}$$

In contrast to $\bar{E}$, the quantity $\eta^*$ is not overlined because it is not defined by a homogenization approach. Please note that
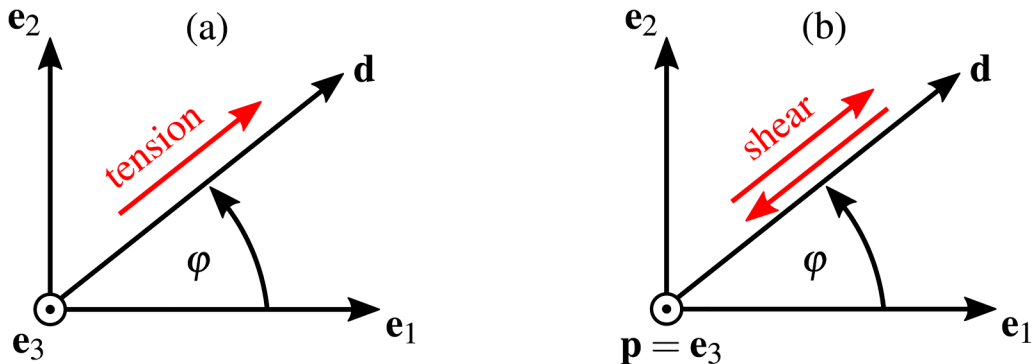


**FIG. 7.** Interpretation of $\mathbf{d}$, $\mathbf{p}$, and $\varphi$ for two different cases: anisotropic stiffness (a) and anisotropic viscosity (b).

all quantities in this section are assumed to be independent of $(\mathbf{x}, t)$ meaning that only stationary and homogeneous microstructures are considered. Moreover, the results are limited to the fiber volume fraction $\phi = 0.1$ and to the aspect ratio $\alpha = 10$. It is pointed out that the latter parameters do not affect the material symmetry, as long as $\phi > 0$ and $\alpha > 1$ hold. Hence, only the impact of $C_I$ is studied in view the given kinematic states. It should be noted that effective Young's modulus is defined on the unit sphere in the 3D space. For a complete graphical visualization of the effective stiffness, the directional-dependent bulk modulus should also be taken into account [46]. In contrast to Young's modulus, the viscosity is defined on the set of rank-one tensors. Therefore, a graphical representation is not given in the 3D space. To circumvent this problem, the shear plane normal $\mathbf{p}$ is fixed and the shear direction $\mathbf{d}$ is varied. Then, one obtains a first insight into the directional-dependent viscosity which is induced by the fiber orientation distribution. It should be noted that the fiber orientation distribution defining the viscous anisotropy is fixed. In consequence, the shown results are not to be interpreted from an experimental point of view, since any shear will cause a reorientation leading to a new anisotropic state. The reason of choosing $\eta^*$ is to show how the used closure predicts the viscous anisotropy for different orientation states (aligned versus more isotropic). As mentioned before, this is the basis of the coupled simulation approach where the suspension flow is affected by the fiber orientation and vice versa.

In Fig. 8, the anisotropic viscous behavior is shown for fiber suspensions with flow-dependent asymptotic orientation states. The parameter $C_I$ is increased within the interval $[10^{-4}, 1]$ (see Sec. IV A). For the compression flow, small values of $C_I$ refer to PI fiber orientation, whereas for all other flows small values of $C_I$ refer to aligned orientation states. The opposite case with large values of $C_I$ is characterized by more isotropic orientation states for all considered flows. As known from previous studies [3,35], aligned fiber orientation states are characterized by a lower shear viscosity compared to the effective shear viscosity of isotropic suspensions. As explained before, $C_I$ can be interpreted as a driving force toward the isotropic orientation, which leads to increased and isotropized shear viscosity.
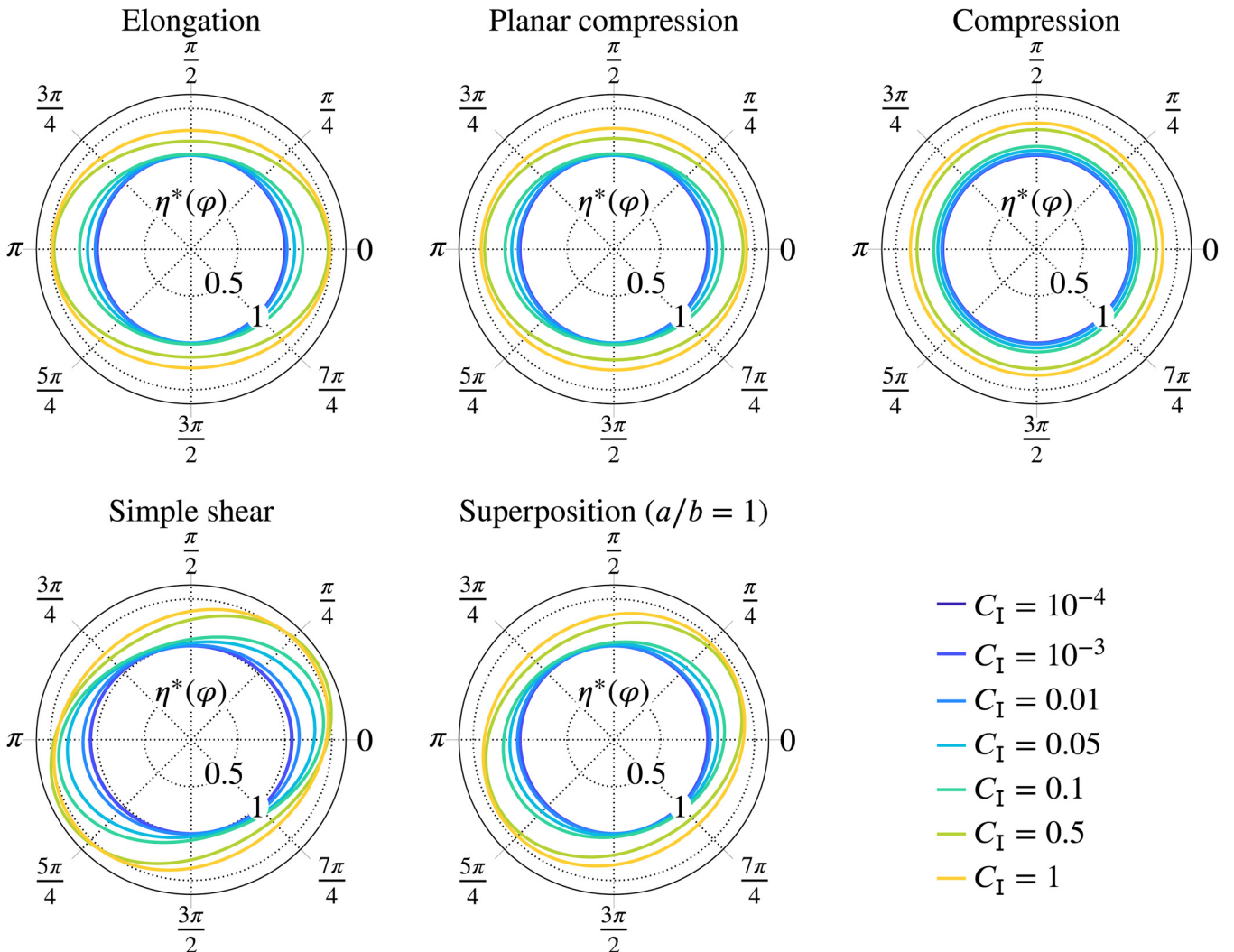


**FIG. 8.** Dimensionless effective shear viscosity of a fiber suspension for different asymptotic orientation states set by the flow kinematics depending on $C_I$ ($\mathbf{e}_1$–$\mathbf{e}_2$-plane, $\phi = 0.1$, $\alpha = 10$, Dinh–Armstrong model, QC).

In Fig. 9, the anisotropic elastic behavior is shown for fiber-reinforced composites with asymptotic orientation states. Similar to the viscosity results, the transition from aligned orientation states to more isotropic fiber orientation is illustrated. For larger values of $C_I$ representing orientation states closer to isotropy, the weakness of the QC overestimating the anisotropy is clearly visible. As a consequence, the QC leads to poor estimations of the effective elastic behavior regarding orientation states deviating from the aligned fiber orientation. Compared to the shear viscosity this weakness is more distinct in case of elasticity. Toward aligned fibers the stiffness prediction based on the QC shows the correct transversely isotropic material symmetry. It is stated out that the weakness of the QC is corrected in Sec. IV D, while maintaining the simple structure of the closure.

## C. Discussion of the QC

In the present section, the benefits and the limits of the QC are discussed. Throughout this study, fourth-order tensors are used in the normalized Voigt notation with the base system $\mathbb{B}_{\iota\gamma} = \mathbf{B}_\iota \otimes \mathbf{B}_\gamma$ and the six orthonormal second-order base tensors $\mathbf{B}_\iota$ ($\iota = 1, \ldots, 6$) defined as follows [46]:

$$
\begin{aligned}
\mathbf{B}_1 &= \mathbf{e}_1 \otimes \mathbf{e}_1, & \mathbf{B}_4 &= \sqrt{2}\,\mathrm{sym}(\mathbf{e}_2 \otimes \mathbf{e}_3), \\
\mathbf{B}_2 &= \mathbf{e}_2 \otimes \mathbf{e}_2, & \mathbf{B}_5 &= \sqrt{2}\,\mathrm{sym}(\mathbf{e}_1 \otimes \mathbf{e}_3), \\
\mathbf{B}_3 &= \mathbf{e}_3 \otimes \mathbf{e}_3, & \mathbf{B}_6 &= \sqrt{2}\,\mathrm{sym}(\mathbf{e}_1 \otimes \mathbf{e}_2).
\end{aligned} \tag{31}
$$

By using Eq. (31), the normalized fourth-order tensor $\mathbb{N}$ reads [46,47]

$$
\mathbb{N} =
\begin{bmatrix}
N_{1111} & N_{1122} & N_{1133} & \sqrt{2}N_{1123} & \sqrt{2}N_{1113} & \sqrt{2}N_{1112} \\
 & N_{2222} & N_{2233} & \sqrt{2}N_{2223} & \sqrt{2}N_{2213} & \sqrt{2}N_{2212} \\
 & & N_{3333} & \sqrt{2}N_{3323} & \sqrt{2}N_{3313} & \sqrt{2}N_{3312} \\
 & & & 2N_{2323} & 2N_{2313} & 2N_{2312} \\
 & & & & 2N_{1313} & 2N_{1312} \\
\text{sym} & & & & & 2N_{1212}
\end{bmatrix} \mathbb{B}_{\iota\gamma} =
\begin{bmatrix}
N_{1111} & N_{1122} & N_{1133} & \sqrt{2}N_{1123} & \sqrt{2}N_{1113} & \sqrt{2}N_{1112} \\
 & N_{2222} & N_{2233} & \sqrt{2}N_{2223} & \sqrt{2}N_{2213} & \sqrt{2}N_{2212} \\
 & & N_{3333} & \sqrt{2}N_{3323} & \sqrt{2}N_{3313} & \sqrt{2}N_{3312} \\
 & & & 2N_{2233} & 2N_{3312} & 2N_{2213} \\
 & & & & 2N_{1133} & 2N_{1123} \\
\text{sym} & & & & & 2N_{1122}
\end{bmatrix} \mathbb{B}_{\iota\gamma}. \tag{32}
$$

The first right-hand side of Eq. (32) refers to the standard normalized Voigt notation of fourth-order tensors having both minor and the main symmetry leading to 21 independent components in case of maximum anisotropy [46]. Using the full index symmetry of $\mathbb{N}$ the second right-hand side of Eq. (32) can be formulated with respect to 14 independent components in case of maximum anisotropy. Both right-hand sides differ in how to apply the QC

$$
N_{1212} \approx N_{12}N_{12} \neq N_{11}N_{22} \approx N_{1122}. \tag{33}
$$

Therefore, both right-hand sides induce a different error, which also depends on the orientation state, regarding the index symmetry which cannot be avoided when the QC is used. Throughout this work the second right-hand side of Eq. (32) is used. In the following, the exact orientation states are explored to assess the error induced by the QC

$$
\begin{aligned}
\mathbb{N}_{\mathsf{UD}} &= \mathbf{e}_1 \otimes \mathbf{e}_1 \otimes \mathbf{e}_1 \otimes \mathbf{e}_1, \quad \mathbb{N}_{\mathsf{ISO}} = \frac{1}{3}\mathbb{P}_1 + \frac{2}{15}\mathbb{P}_2, \\
\mathbb{N}_{\mathsf{PI}} &= \frac{3}{8}(\mathbf{e}_1^{\otimes 4} + \mathbf{e}_2^{\otimes 4}) + \frac{1}{8}(\mathbf{e}_1^{\otimes 2} \otimes \mathbf{e}_2^{\otimes 2} + \mathbf{e}_2^{\otimes 2} \otimes \mathbf{e}_1^{\otimes 2}) \\
&\quad + \frac{1}{8}\mathbf{e}_1 \otimes \mathbf{e}_2 \otimes \mathbf{e}_1 \otimes \mathbf{e}_2.
\end{aligned} \tag{34}
$$

Please note that the tensors given in Eq. (34) have to be transformed to the normalized Voigt notation. The closure input $\mathbf{N}$ related to $\mathbb{N}$ given in Eq. (34) is as follows:

$$
\mathbf{N}_{\mathsf{UD}} = \mathbf{e}_1^{\otimes 2}, \quad \mathbf{N}_{\mathsf{ISO}} = \frac{1}{3}\mathbf{I}, \quad \mathbf{N}_{\mathsf{PI}} = \frac{1}{2}(\mathbf{e}_1^{\otimes 2} + \mathbf{e}_2^{\otimes 2}). \tag{35}
$$

Furthermore, three different experimentally measured fourth-order orientation tensors are used to investigate the error of the QC. In this work, the tensors $\mathbb{N}(0°)$, $\mathbb{N}(45°)$, and $\mathbb{N}(90°)$ are used with the appropriate closure input $\mathbf{N}(0°)$, $\mathbf{N}(45°)$, and $\mathbf{N}(90°)$ of Kehrer et al. [45]. Note that the corresponding components in Table 5 of Kehrer et al. [45] also have to be transformed to the normalized Voigt notation. Only then algebraic operations acting on $\mathbb{N}$ are valid. The following error measure $e(\mathbb{N}_{\mathsf{closure}}, \mathbb{N})$ is used for the closure investigation with $\mathbb{N}$ based on Eq. (34) and on $\mathbb{N}(0°)$, $\mathbb{N}(45°)$, and $\mathbb{N}(90°)$ from Kehrer et al. [45],

$$
e = \frac{\|\mathbb{N}_{\mathsf{closure}}(\mathbf{N}) - \mathbb{N}\|}{\|\mathbb{N}\|}. \tag{36}
$$

For comparison, the invariant-based optimal fitting closure [8] (IBOF) is used and should not be reviewed in the present framework. The IBOF closure is chosen to represent modern closure approaches based on parameter fitting to match the results of PDF level computations. Regarding PDF level computations, the reader is referred to the studies of Mezi et al. [35] and Férec et al. [48]. In Table I, the results corresponding to Eq. (36) are shown for the chosen fiber
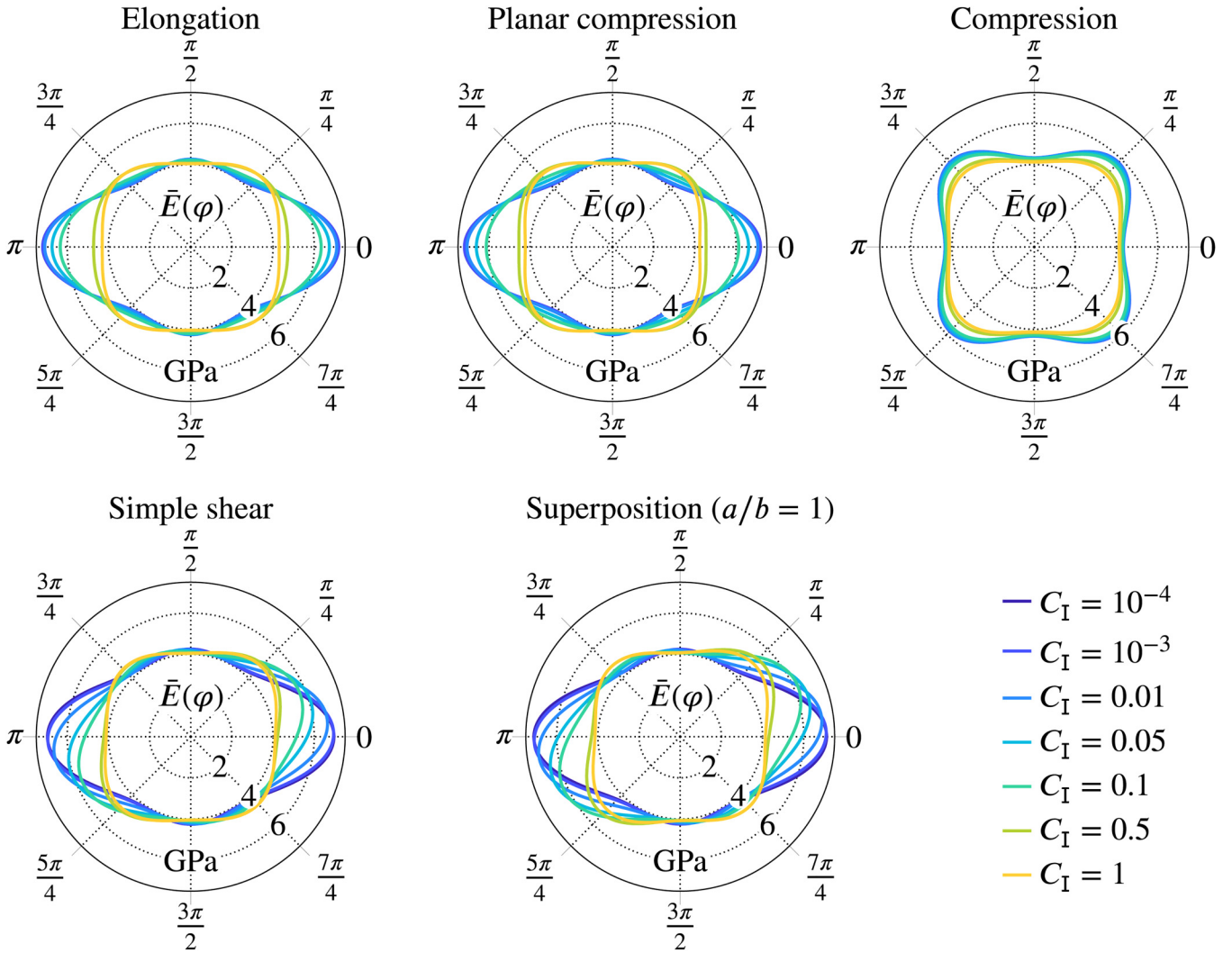
**FIG. 9.** Effective Young's modulus of a fiber-reinforced composite with different asymptotic orientation states set by the flow kinematics depending on $C_I$ ($\mathbf{e}_1$–$\mathbf{e}_2$-plane, $\phi = 0.1$, $\alpha = 10$, MT model, parameters from Appendix H, QC).

orientation states. Please note that Eq. (35) and $\mathbf{N}(0°)$, $\mathbf{N}(45°)$, and $\mathbf{N}(90°)$ are used as closure inputs.

As already known from the literature [49] and as shown in Table I, the QC leads to exact results when the fibers are strictly aligned. When the fiber orientation state turns out to be isotropic or PI, the QC leads to errors which are much larger than for the IBOF closure. In the case of measured fiber orientation states which are close to PI [45] the QC gives errors which are approximately two times larger than

**TABLE I.** Error $e$ concerning QC and IBOF for different fiber orientation states $\mathbb{N}$.

| $\mathbb{N}$ | $e(\mathbb{N}_{QC}, \mathbb{N})$ | $e(\mathbb{N}_{IBOF}, \mathbb{N})$ |
|---|---|---|
| UD | 0.00 | $6.5 \times 10^{-4}$ |
| ISO | 0.54 | $2.2 \times 10^{-15}$ |
| PI | 0.58 | $5.9 \times 10^{-5}$ |
| 0° sample [45] | 0.36 | 0.14 |
| 45° sample [45] | 0.34 | 0.16 |
| 90° sample [45] | 0.38 | 0.16 |

the IBOF-related errors. Compared to the exact orientation states, the difference between these two closures decreased for the measured orientation data.

In contrast to the drawbacks mentioned before, the QC is suitable in the first steps of implementing solvers for fiber suspension flows because it is the simplest approach possible. Furthermore, injection molding parts are often characterized by flat geometries [44], where the fibers tend to align in the flow direction. In such parts, the fiber orientation states are close to the UD case where accuracy of the QC can be evaluated positively. In the context of topology, optimization aligned fiber orientation states are preferred because unloaded material should be removed [50] and the loaded material should be specifically optimized for the known load direction [51].

In the following, the results of two mold filling simulations based on the QC are considered. The domains refer to a simple channel flow (CF) shown in Fig. 10(a) and to a backward-facing step flow (BFS) shown in Fig. 10(b). For more details the reader is referred to Karl *et al.* [3]. The orientation states have been validated based on Eq. (22). In a first step, the Voigt-averaged anisotropic stiffness for both domains is

calculated as follows:

$$\bar{\mathbb{C}}_{\text{domain}} = \frac{1}{V} \sum_{i=1}^{N_{\text{cells}}} V_i \bar{\mathbb{C}}_i^{\text{MT}}. \tag{37}$$

$N_{\text{cells}}$ represents the number of mesh cells used for the mold filling simulations, $V$ stands for the domain volume and $V_i$ characterizes the volume of the $i$th-cell. For every $i$th-cell of the mesh the anisotropic stiffness tensor $\bar{\mathbb{C}}_i^{\text{MT}}$ is determined based on Eq. (27)–(29). Therefore, $\bar{\mathbb{C}}_{\text{domain}}$ refers to a domain-averaged stiffness which can be seen as the true anisotropic elastic behavior of the CF and the BFS part geometry. It should be pointed out that the domains are seen as representative reflecting the expected value of an infinitely large area of this orientation characteristic sufficiently well. Moreover, the domain average Eq. (37) is not unique since, e.g., the harmonic Reuss average also can be used. To show the usefulness of both the QC and the asymptotic states, the idea is to use the asymptotic state of a simple shear flow in areas ① and ② of Figs. 10(a) and 10(b) to estimate $\bar{\mathbb{C}}_{\text{domain}}$ for the CF and the BFS instead of running mold filling simulations. Furthermore, the expensive calculation based on Eq. (37) is avoided.

The red curves in the Figs. 10(c) and 10(d) show the direction dependent Young's modulus averaged over the whole domain for the QC based on Eq. (37). The blue curves refer to the IBOF closure results which are considered as a basis of comparison. The green curves in the Figs. 10(c) and

10(d) represent the effective stiffness of the asymptotic fiber orientation state in the areas ① and ②. The difference between these two areas is the sign of the shear rate leading to an opposite deviation of the eigensystem from the spatial coordinate system. In addition, to take the lower and upper channel kinematics into account the average stiffness of the asymptotic fiber orientation states ① and ② is also considered. It should be stated out that all results shown here refer to a decoupled calculation of fiber orientation and the flow. The following conclusions can be drawn:

- Based on the domain-averaged stiffness the difference between the QC and the IBOF closure is small, which allows us to use the QC combined with a slight correction of the maximum stiffness. The material symmetry does not differ between the two closures.
- The average of the asymptotic state ① and ② leads to the correct material symmetry, while the simplified approach using only ① or ② leads to a slightly rotated anisotropic behavior. A correction is possible subsequently.
- Compared to the domain-averaged case the asymptotic states overestimate the stiffness in $\mathbf{e}_1$-direction. This is caused by neglecting the fiber orientation in area ③ by using the asymptotic fiber orientation in the wall region. In ③, the fiber orientation is either mainly isotropic [Fig. 10(a)] or perpendicular to $\mathbf{e}_1$ [Fig. 10(b)]. By knowing this, the results of the suggested simplified approach can be corrected for a conservative dimensioning.
- The results show that when the dominant fiber orientation state is known based on the geometry and on simplified



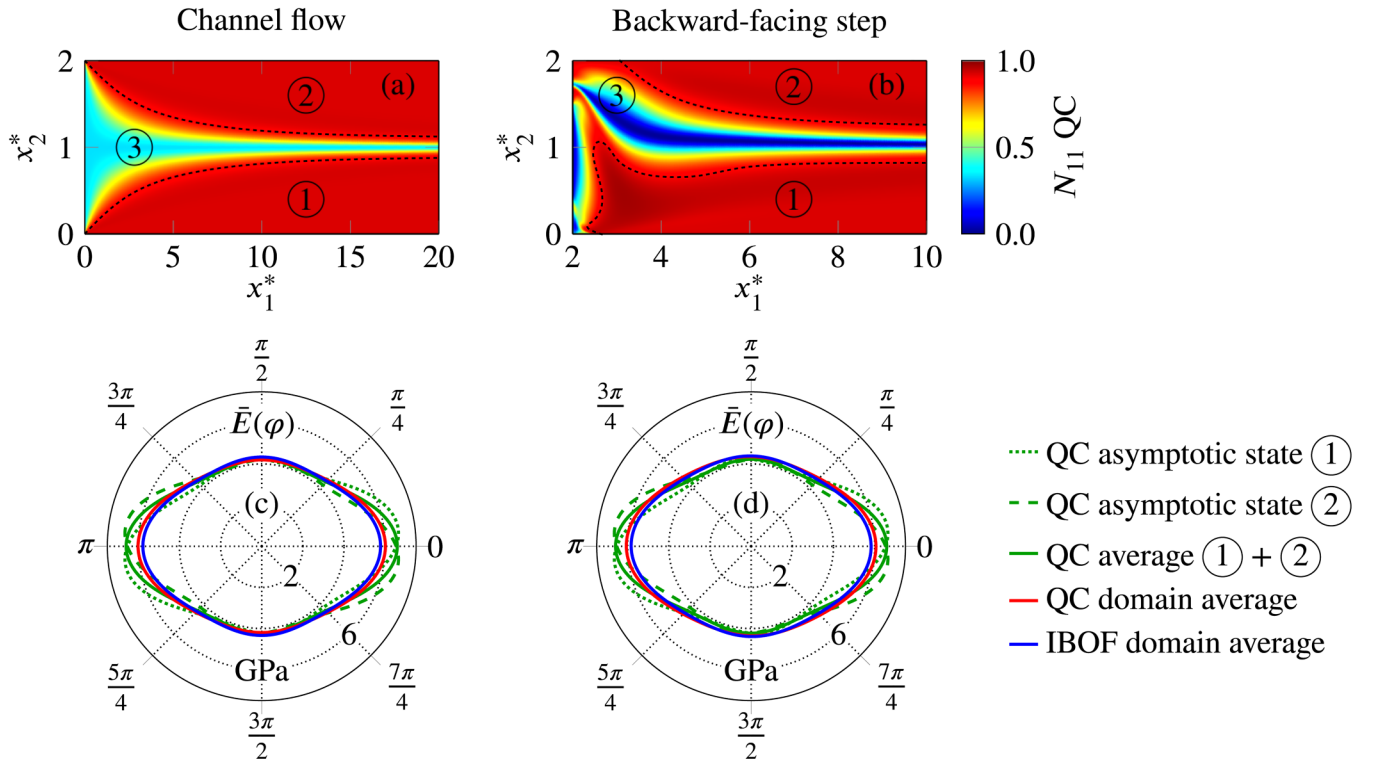**FIG. 10.** Fiber orientation $N_{11}$ in $\mathbf{e}_1$-direction and effective Young's modulus for the QC Voigt-averaged over the domains (channel and backward-facing step geometry [3]) and the approximation with the asymptotic state for the simple shear flow. The IBOF results are shown as a basis of comparison ($\mathbf{e}_1$–$\mathbf{e}_2$-plane, $\phi = 0.1$, $\alpha = 10$, $C_I = 0.01$, MT model, parameters from Appendix H).

**TABLE II.** Error $e$ concerning QC, symQC, and IBOF for different fiber orientation states $\mathbb{N}$.

| $\mathbb{N}$ | $e(\mathbb{N}_{\mathsf{QC}}, \mathbb{N})$ | $e(\mathbb{N}_{\mathsf{symQC}}, \mathbb{N})$ | $e(\mathbb{N}_{\mathsf{IBOF}}, \mathbb{N})$ |
|---|---|---|---|
| UD | 0.00 | 0.00 | $6.5 \times 10^{-4}$ |
| ISO | 0.54 | $2.3 \times 10^{-16}$ | $2.2 \times 10^{-15}$ |
| PI | 0.58 | $9.1 \times 10^{-17}$ | $5.9 \times 10^{-5}$ |
| 0° sample [45] | 0.36 | 0.22 | 0.14 |
| 45° sample [45] | 0.34 | 0.20 | 0.16 |
| 90° sample [45] | 0.38 | 0.20 | 0.16 |

flow conditions, the mechanical behavior can be approximated by using the corresponding asymptotic state.

- The QC can be seen as a compromise between errors associated with the simplicity and the existence of exact expressions for simplified quick estimates. Judged by the simplicity, the QC can be evaluated as a suitable method.

### D. Improvement of the QC by symmetrization

The limitations of the QC are discussed in Secs. IV B and IV C and shown in Figs. 8 and 9 are overcome in the current section by developing and evaluating an improved QC, which is named symQC. This closure is developed in two versions, the former delivering better predictions of the mechanical properties, the latter of flow-induced orientation evolution. Based on one term within the generalized hybrid closure introduced by Petty *et al.* [52], the first correction step contains the symmetrization of $\mathbf{N} \otimes \mathbf{N}$ ensuring the complete index symmetry (symmetric in all index pairs)

$$\mathrm{sym}(\mathbf{N} \otimes \mathbf{N}) = \frac{1}{3}\left(\mathbf{N} \otimes \mathbf{N} + \mathbf{N}\square\mathbf{N} + (\mathbf{N}\square\mathbf{N})^{\mathsf{T}_\mathsf{R}}\right). \quad (38)$$

Based on Eq. (38) the second correction step is defined by normalizing Eq. (38) in such a way that the trace condition $\mathrm{tr}(\mathbb{N}_{\mathsf{symQC}}) = \mathbb{N}_{\mathsf{symQC}} \cdot \mathbb{I} = 1$ is fulfilled leading to the first version of symQC,

$$\mathbb{N}_{\mathsf{symQC}} = \frac{\mathrm{sym}(\mathbf{N} \otimes \mathbf{N})}{\frac{1}{3}(1 + 2\|\mathbf{N}\|^2)}. \quad (39)$$
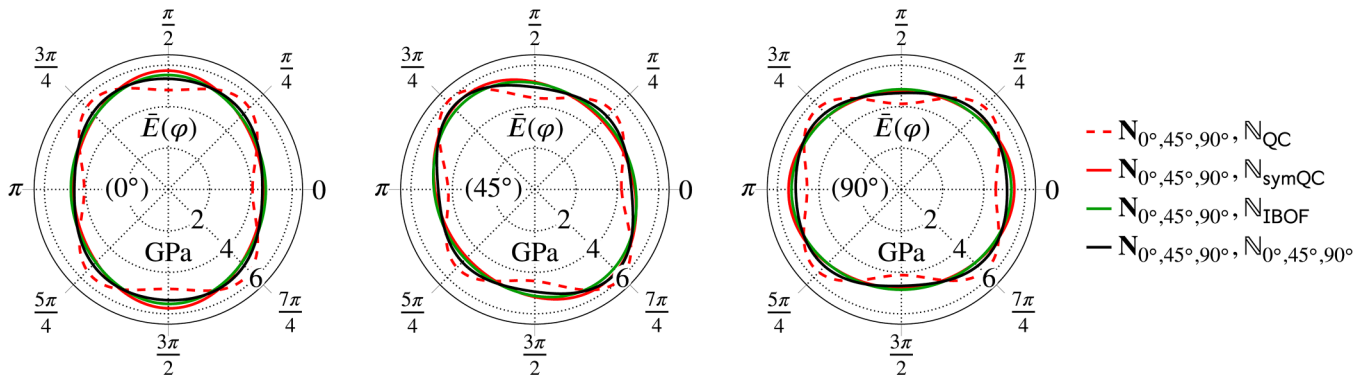
To the best of the authors' knowledge, this closure approach has not been published yet. It is pointed out that compared to the original QC the following basic properties listed in Petty *et al.* [52] have been lost at the cost of the two correction steps already described:

$$\mathbb{N}_{\mathsf{symQC}}[\mathbf{I}] \neq \mathbf{N}, \quad \mathrm{tr}(\mathbb{N}_{\mathsf{symQC}}[\mathbf{D}]) \neq \mathbf{D} \cdot \mathbf{N}. \quad (40)$$

In the framework of estimating the effective anisotropic behavior based on given orientation states $\mathbf{N}$, the complete index symmetry and the trace condition are more important than fulfilling Eq. (40). It is clarified that for exact tensors $\mathbf{N}$ and $\mathbb{N}$, the trace conditions $\mathrm{tr}(\mathbb{N}) = 1$ and $\mathrm{tr}(\mathbf{N}) = 1$ are connected as follows by using the complete index symmetry of $\mathbb{N}$ and the property $\mathbb{N}[\mathbf{I}] = \mathbf{N}$:

$$\mathrm{tr}(\mathbb{N}) = \mathbb{N} \cdot \mathbb{I} = N_{ijkl}\delta_{ik}\delta_{lj} = N_{ijij} = N_{iijj} = \mathbf{I} \cdot \mathbb{N}[\mathbf{I}]$$
$$= \mathbf{I} \cdot \mathbf{N} = \mathrm{tr}(\mathbf{N}) = 1. \quad (41)$$

This is not the case for symQC since $\mathbb{N}_{\mathsf{symQC}}[\mathbf{I}] \neq \mathbf{N}$. Please note that the closure $\mathbb{N}_{\mathsf{symQC}}$ given in Eq. (39) cannot be used within the FTE, since $\mathrm{tr}(\dot{\mathbf{N}}) = 0$ is violated. For that reason, $\mathbb{N}_{\mathsf{symQC}}$ is a method to calculate $\mathbb{N}$ based on a given $\mathbf{N}$ subsequently and refers to the well-known closure procedure compactly written down as a fourth-order tensor function $\mathbb{N} \approx \mathbb{F}(\mathbf{N})$.

In the following, the quality of $\mathbb{N}_{\mathsf{symQC}}$ is investigated by considering the orientation states given in Sec. IV C. The closure-induced error $e(\mathbb{N}_{\mathsf{closure}}, \mathbb{N})$ defined in Eq. (36) is given in Table II. Based on the results a significant improvement of the original QC can be identified for all considered example orientation states. For all analytically given orientation states, symQC leads to smaller errors compared to the IBOF closure.

To illustrate the quality of symQC compared to QC and IBOF, the direction dependent Young's modulus is shown in Fig. 11 based on the measured data of Kehrer *et al.* [45]. Analogously, the MT method is used with the material parameters listed in Appendix H. The black curves refer to the measured fiber orientation data $\mathbf{N}$ and $\mathbb{N}$ [45] as direct input of the stiffness prediction. The other curves represent the stiffness predictions based on the measured $\mathbf{N}$ [45] and

**FIG. 11.** Comparison of QC, symQC, and IBOF in view of the effective Young's modulus defined by the fiber orientation states given in Kehrer *et al.* [45] ($\mathbf{e}_1$–$\mathbf{e}_2$-plane, $\phi = 0.1$, $\alpha = 10$, MT model, parameters from Appendix H).

three different closure methods for approximating $\mathbb{N}$. The results show that there are only small differences between symQC and IBOF, whereas symQC is superior to the IBOF in terms of implementation and computational effort.

Analogous to Sec. IV B, the effective viscous and elastic anisotropy based on symQC is shown in Figs. 12 and 13. Please note that the asymptotic orientation states $\mathbf{N}$ based on QC are used as an input for the improved closure symQC to obtain subsequently enhanced results. Whereas the material symmetry of the viscous behavior in Fig. 12 does not change, the shear viscosity is smaller compared to QC in Fig. 8. This is caused by the symmetrization which can be seen as an average over all involved indices. For the given asymptotic states, this lowers the corresponding entries in $\mathbb{N}_{symQC}$ compared to $\mathbb{N}_{QC}$ since there are vanishing components $N_{ij}$. The material symmetry concerning the effective elastic anisotropy in Fig. 13 changes in the sense that the transition from aligned to more isotropic orientation states is correctly processed by symQC. To conclude this section, it is pointed out that using symQC does not lead to significantly improved results in the framework of the estimation method

shown in Fig. 10. The reason being that in CF and BFS, aligned fiber orientation states dominate which are already correctly handled by QC. When the closure implementation should be kept simple the use of symQC is suggested instead of QC justified by the results in this paper. It should be repeated that $\mathbb{N}_{symQC}$ given in Eq. (39) cannot be used within the FTE, since $\mathrm{tr}(\dot{\mathbf{N}}) = 0$ is violated.

The second version of symQC is developed in order to be used in the FTE describing the fiber orientation evolution. In contrast to the first version of symQC, the second version approximates the linear mapping $\mathbb{N}[\mathbf{D}]$ appearing in the FTE. By using a general function $\mathbf{G}$ this closure scheme reads $\mathbb{N}[\mathbf{D}] \approx \mathbf{G}(\mathbf{N}, \mathbf{D})$. One important property is that $\mathbb{N}$ can only be computed independently of $\mathbf{D}$, if $\mathbf{G}$ is linear in $\mathbf{D}$. In all other cases, $\mathbb{N}$ depends on the deformation process. The current approach of approximating $\mathbb{N}[\mathbf{D}]$ has been pursued already by Hinch and Leal [53], who distinguish between strong (isotropic states, $C_I$ large) and small (aligned states, $C_I$ small) fiber-fiber interactions. They obtain the so-called composite closure by approximating these two extreme alignment states via an interpolation. Advani and Tucker [6] provide a comprehensive
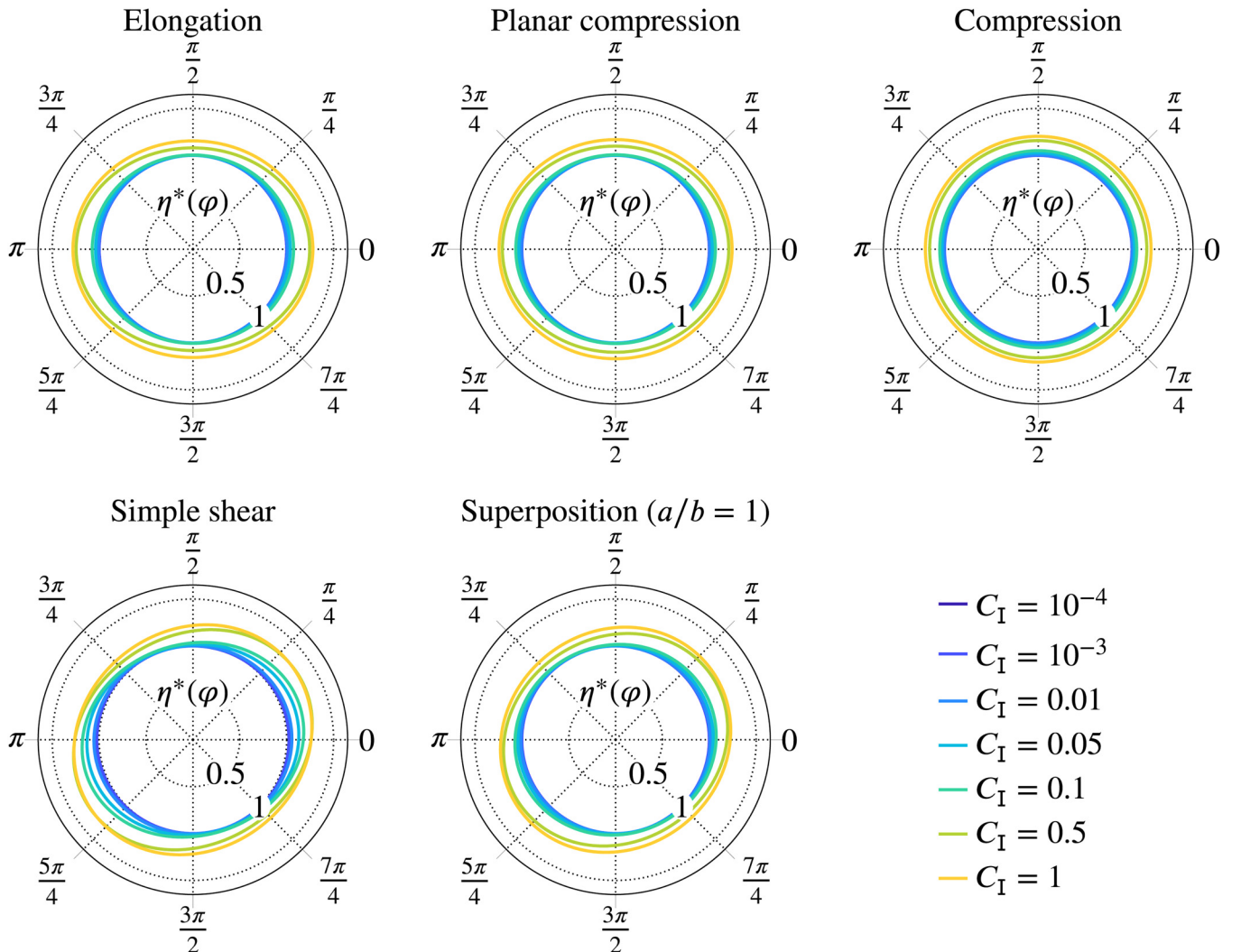


**FIG. 12.** Dimensionless effective shear viscosity of a fiber suspension for different asymptotic orientation states set by the flow kinematics depending on $C_I$ ($\mathbf{e}_1$–$\mathbf{e}_2$-plane, $\phi = 0.1$, $\alpha = 10$, Dinh–Armstrong model, symQC).
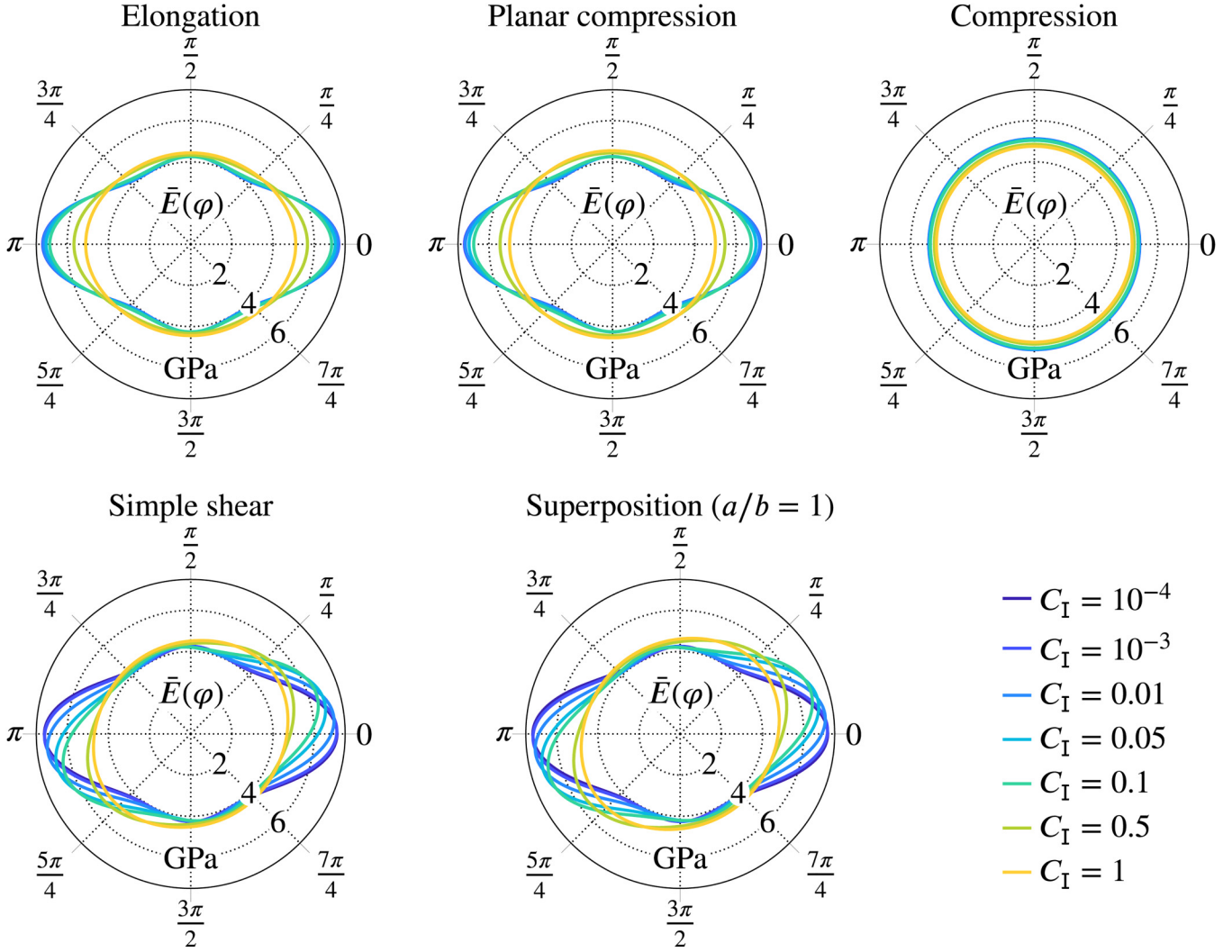
**FIG. 13.** Effective Young's modulus of a fiber-reinforced composite with different asymptotic orientation states set by the flow kinematics depending on $C_I$ ($e_1$–$e_2$-plane, $\phi = 0.1$, $\alpha = 10$, MT model, parameters from Appendix H, symQC).

description of such closures, which approximate $\mathbb{N}[\mathbf{D}]$ instead of $\mathbb{N}$. It is noted that $\mathbb{N}[\mathbf{D}]$ does not only occur in the FTE but also occur in the Dinh–Armstrong model [17], Eq. (26) predicting the anisotropic viscous behavior of fiber suspensions. As a consequence, using the scheme $\mathbb{N}[\mathbf{D}] \approx \mathbf{G}(\mathbf{N}, \mathbf{D})$ the influence of the deformation process on the viscous anisotropy is improved representing the flow-fiber coupling.

The procedure of finding the closure function $\mathbf{G}(\mathbf{N}, \mathbf{D})$ preserving $\text{tr}(\mathbf{N}) = 1$ in the context of symQC is given in Appendix I. The idea is to introduce a scalar factor $\kappa(\mathbf{N}, \mathbf{D})$ in front of the closure term in the FTE. The quantity $\kappa$ is determined by forcing $\text{tr}(\dot{\mathbf{N}}) = 0$. Based on the analysis shown in Appendix I, the following expression holds for $\kappa$ depending on the local flow and orientation state:

$$\kappa = \begin{cases} 0, & \mathbf{N} = \mathbf{N}_{\text{ISO}} \text{ and/or } \mathbf{D} = \mathbf{0}, \\ \dfrac{6\,\mathbf{N} \cdot \mathbf{D}}{\mathbf{N} \cdot \mathbf{D} + 2\mathbf{D} \cdot \mathbf{N}^2}, & \mathbf{N} \neq \mathbf{N}_{\text{ISO}}, \mathbf{D} \neq \mathbf{0}. \end{cases} \quad (42)$$

It should be noted that $\kappa$ is a homogeneous function of degree 0 in $\mathbf{D}$. Furthermore, $\kappa$ only depends on the direction

of $\mathbf{D}$ and not on the magnitude $\|\mathbf{D}\|$. Since the normalization factor used in Eq. (39) cancel out as shown in Appendix I, the FTE with symQC and $\kappa$ defined in Eq. (42) reads

$$\begin{aligned} \dot{\mathbf{N}} &= \mathbf{W}\mathbf{N} - \mathbf{N}\mathbf{W} + \xi\Big(\mathbf{D}\mathbf{N} + \mathbf{N}\mathbf{D} - \kappa\,\text{sym}(\mathbf{N} \otimes \mathbf{N})[\mathbf{D}]\Big) \\ &\quad + 2C_I\dot{\gamma}(\mathbf{I} - 3\mathbf{N}) \\ &= \mathbf{W}\mathbf{N} - \mathbf{N}\mathbf{W} + \xi\Big(\mathbf{D}\mathbf{N} + \mathbf{N}\mathbf{D} - \frac{\kappa}{3}(\mathbf{N} \cdot \mathbf{D})\mathbf{N} - \frac{2\kappa}{3}\mathbf{N}\mathbf{D}\mathbf{N}\Big) \\ &\quad + 2C_I\dot{\gamma}(\mathbf{I} - 3\mathbf{N}). \end{aligned} \quad (43)$$

Detailed information concerning the case distinction of $\kappa$ can be found in Appendix I. To the best of the authors knowledge, this closure approach has not been published yet. Please note that only incompressible flows are considered. It should be pointed out that asymptotic states based on Eq. (43) are not investigated. On the one hand, the asymptotic representation of Eq. (43) does not lead to manageable exact expressions. On the other hand, numerically generated
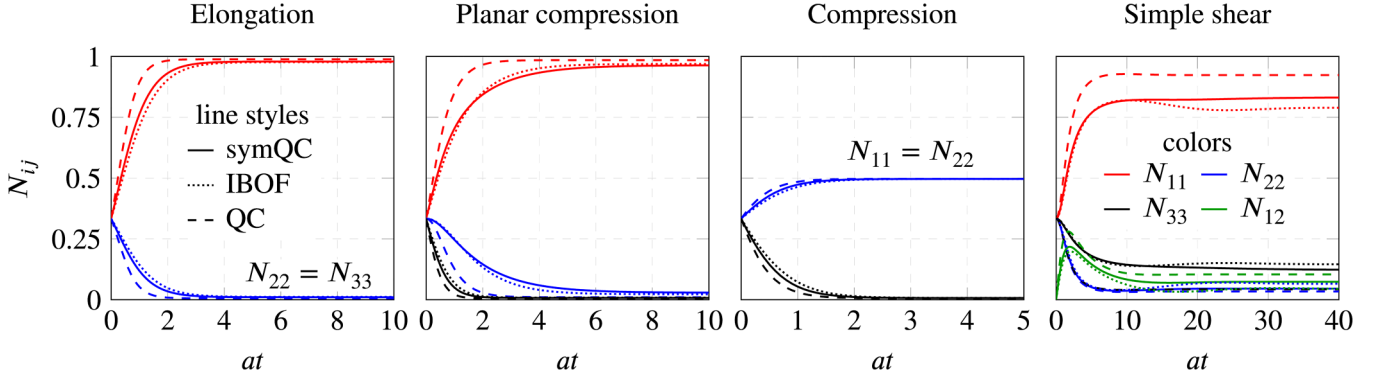
**FIG. 14.** Comparison of $N_{ij}$ over the total deformation $at$ for four different homogeneous flows using QC, symQC and IBOF integrated explicitly with a 4th-order Runge–Kutta method ($\alpha = 10$, $C_1 = 0.01$, $\triangle t = 10^{-2}$ s).

asymptotic solutions do not provide novel information compared to Figs. 3 and 4.

The performance of symQC within the FTE is shown in Fig. 14 for the spin-free flows and the simple shear flow given in Secs. III B and III C. For comparison, the results referring to the QC and to the IBOF closure are given additionally. Since the flows are homogeneous, the FTE is an ordinary differential equation for **N** which is integrated with a 4th-order Runge–Kutta method [54] within this study. The components $N_{ij}$ are plotted against the dimensionless deformation $at$ with the deformation rate $a$ defined for each flow in Secs. III B and III C. The results refer to $\alpha = 10$ and $C_1 = 0.01$ and show that symQC improves the results of QC significantly if the IBOF-related results are seen as an evaluation basis. To conclude this section, the results of a simple shear flow regarding $\alpha \to \infty$ and $C_1 = 0.01$ are shown in Fig. 15. The spin-free flows are not shown, as there is no optically recognizable difference in the results referring to $\alpha = 10$ and $\alpha \to \infty$. One can see that the quality of the symQC-predicted orientation state has improved for $\alpha \to \infty$ compared to Fig. 14.

### E. Improvement of the QC by adopting $C_1$

By looking at the simple shear flow results in Fig. 14, the following question arises: How to correct $C_1$ for the QC to achieve the asymptotic state of the IBOF closure? In the following, the parameter $C_{1,QC}$ refers to the interaction parameter regarding the analytical expressions of this paper. On the other hand, $C_{1,IBOF}$ refers to the interaction parameter in the context of the IBOF-closed FTE solved for the simple shear flow. The idea is to connect $C_{1,QC}$ with $C_{1,IBOF}$ for the shear flow in order to improve the analytical and numerical prediction of **N** based on the QC. This is done by solving the following equation numerically for $C_{1,QC}$ with given $\alpha$ and $C_{1,IBOF}$:

$$N_{11}(C_{1,IBOF}) = \frac{(\xi + 1)\psi + C_{1,QC}}{2\xi\psi + 3C_{1,QC}}. \qquad (44)$$

Please note that $\psi$ is given in Eq. (F3) depending on $\alpha$ via $\xi$ and on $C_{1,QC}$. In Eq. (44), $N_{11}(C_{1,IBOF})$ refers to the asymptotic solution based on the IBOF closure and on $C_{1,IBOF}$. The results are plotted in Fig. 16 and show how to choose $C_{1,QC}$ with respect to $C_{1,IBOF}$ to get the IBOF-predicted asymptotic shear flow solution by using the QC. In general, $C_{1,QC} > C_{1,IBOF}$ holds since the QC requires a larger interaction forcing to match the IBOF results lying closer to the isotropic orientation state.
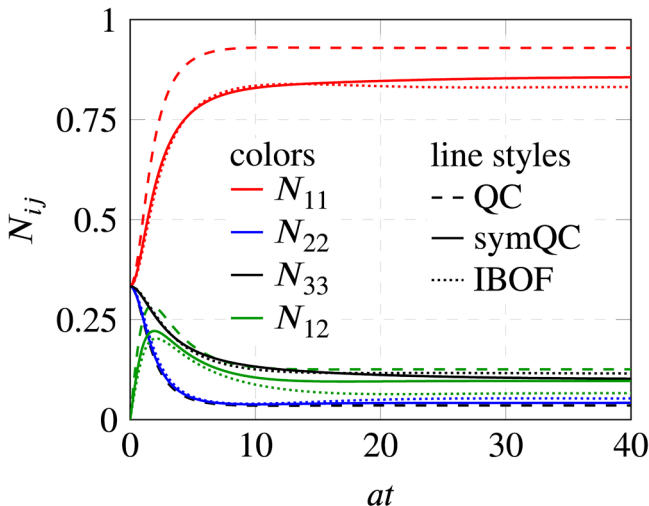


**FIG. 15.** $N_{ij}$ over the total deformation $at$ for the simple shear flow using QC, symQC, and IBOF integrated explicitly with a 4th-order Runge–Kutta method ($\alpha \to \infty$, $C_1 = 0.01$, $\triangle t = 10^{-2}$ s).
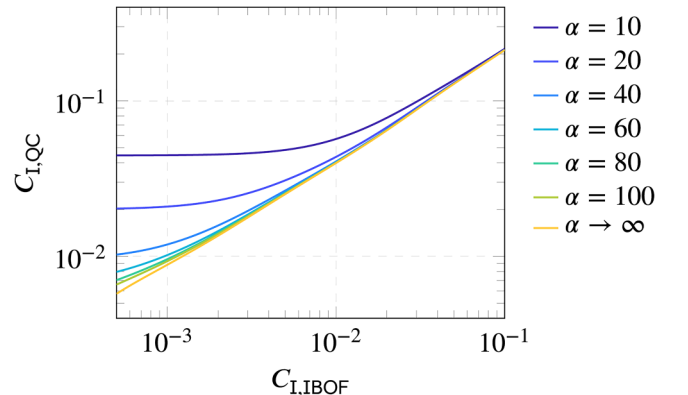


**FIG. 16.** $C_{1,QC}$ plotted over $C_{1,IBOF}$ to generate the IBOF asymptotic orientation state by using the QC (limited to simple shear flow).

In summary, the second improvement of the QC does not operate on the closure itself as done in Sec. IV D. This improvement is not meant to be used to reconstruct $\mathbb{N}$ by using $\mathbf{N}$. Rather, the fiber interaction within the quadratically closed FTE is corrected by using the asymptotic IBOF solution in a simple shear flow for different fiber aspect ratios. The advantage of this method is that the QC within the FTE and the analytical expressions in Sec. III still can be used.

## V. SUMMARY AND CONCLUSION

In the present study, exact solutions of the quadratically closed FTE [4,13] regarding simple flows are presented and investigated in the general framework of asymptotic behavior. In contrast to existing exact solutions, which only take into account flow state and fiber geometry [14,29], the present algebraic expressions also consider the fiber-fiber interaction. The study is limited to laminar and incompressible fiber suspension flows with rigid fibers suspended in a Newtonian fluid. Any external and internal forces are not considered. Furthermore, the exact expressions refer to homogeneous simple shear, elongational and two compression flows which can be interpreted as local kinematic states within complex flows. The asymptotic orientation states illustrate the nonlinear influence of $\alpha$ and $C_I$. The asymptotic fiber orientation states with QC in use are discussed in terms of viscous and elastic anisotropy. The results show that the error in material symmetry concerning the anisotropic stiffness is more distinct compared to viscous anisotropy considerations. The models of Dinh and Armstrong [17] and of Mori and Tanaka [18,43] are used combined with an OA scheme [4]. A simple procedure estimating the stiffness of flat injection molding parts is provided using the QC and the asymptotic state of a simple shear flow. The recognized disadvantages of QC are improved by postulating a normalized fully symmetric QC (first version of symQC) enhancing the predicted material symmetry. This approach is validated by comparing the results with IBOF-related predictions. Furthermore, the introduced closure keeps the simple structure and turns out to be a fast and accurate method estimating the anisotropic behavior of fiber suspensions and fiber-reinforced composites. An adaption of the new closure is developed for using it within the FTE (second version of symQC). In this context, an additional scalar parameter depending on the local orientation and kinematic state is introduced. The result is a simple closure function approach depending on the deformation process which relies on the idea, originally introduced by Hinch and Leal [6,53], of approximating $\mathbb{N}[\mathbf{D}]$ instead of $\mathbb{N}$. By using an explicit integration scheme, the improvement of the QC within the FTE is demonstrated in simple flows. In addition, a method improving the asymptotic fiber orientation prediction is introduced by using the common QC and optimized fiber-fiber interaction parameter values.

## VI. OUTLOOK

In this section, a brief outlook is given on how the asymptotic FTE (10) can be used in the framework of reverse engineering. The common engineering approach is to determine the resulting fiber orientation of a given process. However, from an inverse engineering point of view, the process conditions should be varied to generate desired anisotropic composite properties. Based on the fact that many kinematic input quantities influence the anisotropic microstructural state, this is a nontrivial task.

Since the fiber orientation state based on the FTE (5) depends on $\alpha$, $C_I$, and the closure $\mathbb{F}(\mathbf{N})$ in use, the reverse engineering procedure faces various difficulties. For clarity, the reverse engineering procedure means setting $\mathbf{N}$, $\alpha$, $C_I$, and the closure $\mathbb{F}(\mathbf{N})$ for calculating the kinematic quantities $\mathbf{D}$ and $\mathbf{W}$. Unfortunately, this problem formulation first is underdetermined due to six equations for $N_{ij}$ at hand (FTE) to calculate nine unknown $D_{ij}$ and $W_{ij}$. To ensure a clear solvability, three additional equations have to be formulated regarding kinematical restrictions. For the special case of incompressible flows, $\mathrm{tr}(\mathbf{D}) = 0$ can be used. Additionally, $\|\mathbf{D}\|$ and $\|\mathbf{W}\|$ can be forced taking on desired values. As mentioned before, the space of possible solutions $N_{ij}$ is also defined by $\alpha$, $C_I$, and the closure $\mathbb{F}(\mathbf{N})$ besides the deformation process. Strictly speaking, this means that further equations for $\alpha$, $C_I$, and $\mathbb{F}(\mathbf{N})$ are necessary, which leads to an over-determined system for $N_{ij}$. The dependence of the solution space on $\alpha$, $C_I$, and $\mathbb{F}(\mathbf{N})$ cannot be identified by separate equations since this information is intrinsically given in the FTE. Therefore, it is not certain that a mathematically correct desired $N_{ij}$ is an element of the multidimensional solution space, describing an asymptotic state in the context of the chosen parameters.

The asymptotic FTE (10) can be used in order to minimize the computational cost, since the material time derivative of $\mathbf{N}$ is neglected. This simplification means that only the influence of $\mathbf{D}$ and $\mathbf{W}$ on the equilibrium orientation state is considered. Nevertheless, the aforementioned difficulties are still unsolved. A pragmatic approach would be to choose many values $D_{ij}$ and $W_{ij}$ of interest and solve for the corresponding $\mathbf{N}$ for fixed $\alpha$, $C_I$, and a given closure $\mathbb{F}(\mathbf{N})$. Since multiple solutions exist generally, the physically sensible solution $\mathbf{N}$ is to be found by checking for the correct algebraic properties. Please note that, strictly speaking, this procedure is no longer reverse engineering but has the advantage of determining a lot of combinations $\{\mathbf{D}, \mathbf{W}, \mathbf{N}\}$. As a consequence, the conclusion $\mathbf{N} \rightarrow \{\mathbf{D}, \mathbf{W}\}$ can be drawn.

The inverse problem of designing microstructures for a defined performance also occurs in the application of metals [55]. The method shown is extended by Shaffer *et al.* [56] to be applied to process design identifying deformation paths leading to load-optimized microstructures.

## APPENDIX A: SECOND- AND THIRD-KIND ORIENTATION TENSORS

Orientation tensors of the second kind with arbitrary even order $n$ are denoted by $\mathbb{N}^{(2)}_{\langle n \rangle}(\mathbf{x}, t)$ and are defined by [5,34]

$$\int_{\mathscr{S}}\left(\mathbb{N}_{\langle n\rangle}^{(2)}\cdot\mathbf{n}^{\otimes n}-f\right)^2 \mathrm{d}S \to \min. \tag{A1}$$

This means that orientation tensors of the second kind minimize the approximation error against the true PDF in an integral sense [5]. The general definition is as follows [5]:

$$\mathbb{N}_{\langle n\rangle}^{(2)} = \frac{2n+1}{2^n}\binom{2n}{n}\left[\mathbb{N}_{\langle n\rangle}^{(1)} + a_{n-2}^n\mathrm{sym}(\mathbf{I}\otimes\mathbb{N}_{\langle n-2\rangle}^{(1)})\right.$$
$$\left. + a_{n-4}^n\mathrm{sym}(\mathbf{I}^{\otimes 4}\otimes\mathbb{N}_{\langle n-4\rangle}^{(1)}) + \cdots + a_0^n\mathrm{sym}(\mathbf{I}^{\otimes n})\right]. \tag{A2}$$

The operation sym($\cdot$) refers to a complete symmetrization concerning all indices [57]. The orientation tensors of the third kind $\mathbb{N}_{\langle n\rangle}^{(3)}(\mathbf{x}, t)$ are defined as follows and represent symmetric traceless (deviatoric) tensors [5,34],

$$\mathbb{N}_{\langle n\rangle}^{(3)} = \frac{2n+1}{2^n}\binom{2n}{n}\mathbb{N}_{\langle n\rangle}^{(1)'}. \tag{A3}$$

The deviatoric part $\mathbb{N}_{\langle n\rangle}^{(1)'}$ of the first-kind orientation tensor of arbitrary even order $n$ can be determined as follows [5]:

$$\mathbb{N}_{\langle n\rangle}^{(1)'} = c_0^n\mathbb{N}_{\langle n\rangle}^{(1)} + c_2^n\mathrm{sym}(\mathbf{I}\otimes\mathbb{N}_{\langle n-2\rangle}^{(1)}) + c_4^n\mathrm{sym}(\mathbf{I}^{\otimes 4}\otimes\mathbb{N}_{\langle n-4\rangle}^{(1)})$$
$$+ \cdots + c_n^n\mathrm{sym}(\mathbf{I}^{\otimes n}). \tag{A4}$$

The coefficients $c_m^n$ and $a_m^n$ ($n, m$: even) within Eqs. (A2) and (A4) are defined by [5]

$$c_0^n = 1,$$
$$c_m^n = (-1)^{m/2}\binom{n}{m}\binom{n-1}{m/2}\bigg/\binom{2n-1}{m},$$
$$a_m^n = \sum_{\substack{k=m\\k:\text{even}}}^n \frac{2k+1}{2^k}\binom{2k}{k}c_{k-m}^k\bigg/\frac{2n+1}{2^n}\binom{2n}{n}. \tag{A5}$$

## APPENDIX B: SOLUTIONS OF QUADRATIC AND CUBIC EQUATIONS

In this section, the procedure to investigate the solutions of quadratic and cubic equations is summarized in order to make the paper self-contained (see, e.g., Arens *et al.* [58] and Merziger *et al.* [59]). First of all, quadratic equations with the solution variable $\psi$ are considered generally as follows:

$$0 = k_2\psi^2 + k_1\psi + k_0. \tag{B1}$$

The solution of Eq. (B1) depends on the discriminant $D$, which is defined as follows:

$$D = k_1^2 - 4k_2k_0,$$
$$D < 0: \text{two complex solutions,}$$
$$D = 0: \text{one real double solution,} \tag{B2}$$
$$D > 0: \text{two real solutions.}$$

Second, cubic equations with the solution variable $\psi$ are considered generally by

$$0 = k_3\psi^3 + k_2\psi^2 + k_1\psi + k_0,$$
$$\Leftrightarrow 0 = \psi^3 + \tilde{k}_2\psi^2 + \tilde{k}_1\psi + \tilde{k}_0, \tag{B3}$$

where the coefficients are defined by $\tilde{k}_2 = k_2/k_3$, $\tilde{k}_1 = k_1/k_3$, and $\tilde{k}_0 = k_0/k_3$. The latter equation can be rewritten as follows using a change of variable $\tilde{\psi} = \psi + \tilde{k}_2/3$:

$$0 = \tilde{\psi}^3 + p\tilde{\psi} + q, \tag{B4}$$

where the new coefficients $p$ and $q$ are defined as follows:

$$p = \frac{3\tilde{k}_1 - \tilde{k}_2^2}{3}, \quad q = \frac{2\tilde{k}_2^3}{27} - \frac{\tilde{k}_1\tilde{k}_2}{3} + \tilde{k}_0. \tag{B5}$$

The solution of Eq. (B3) depends on the discriminant $D$, which is defined by

$$D = \left(\frac{p}{3}\right)^3 + \left(\frac{q}{2}\right)^2,$$
$$D < 0: \text{three pairwise different real solutions,}$$
$$D = 0: \text{three real solutions (at least two equal),}$$
$$D > 0: \text{one real and two complex solutions.} \tag{B6}$$

The coefficients $k_i$ can be determined by comparing the equations for $\psi$ in Appendixes C–F with Eq. (B1) or (B3), respectively.

## APPENDIX C: ELONGATIONAL FLOW

The following system of Eq. (C1) (given multiplied by 2) is solved exactly for the components $N_{ij}$. Note that equations are given independently of the rate of deformation $a > 0\,\mathrm{s}^{-1}$

$$0 = 2\xi(2N_{11} - (2N_{11} - N_{22} - N_{33})N_{11}) + 2\sqrt{3}C_\mathrm{I}(1 - 3N_{11}),$$
$$0 = 2\xi(N_{12}/2 - (2N_{11} - N_{22} - N_{33})N_{12}) - 6\sqrt{3}C_\mathrm{I}N_{12},$$
$$0 = 2\xi(N_{13}/2 - (2N_{11} - N_{22} - N_{33})N_{13}) - 6\sqrt{3}C_\mathrm{I}N_{13},$$
$$0 = 2\xi(-N_{22} - (2N_{11} - N_{22} - N_{33})N_{22}) + 2\sqrt{3}C_\mathrm{I}(1 - 3N_{22}),$$
$$0 = 2\xi(-N_{23} - (2N_{11} - N_{22} - N_{33})N_{23}) - 6\sqrt{3}C_\mathrm{I}N_{23},$$
$$0 = 2\xi(-N_{33} - (2N_{11} - N_{22} - N_{33})N_{33}) + 2\sqrt{3}C_\mathrm{I}(1 - 3N_{33}). \tag{C1}$$

The parameter $\psi$ describing the orientation state in Eq. (16) can be obtained by solving the following equation:

$$0 = \xi\psi^2 + (\sqrt{3}C_\mathrm{I} - \xi)\psi - \frac{\sqrt{3}}{3}C_\mathrm{I}. \tag{C2}$$

In Fig. 17, the discriminant $D$ is shown depending on the parameters $\alpha$ and $C_\mathrm{I}$ (see Appendix B). It can be seen that $D > 0$ holds resulting in two real solutions for $\psi$. The only physically meaningful solution $\psi$ of Eq. (C2) is as follows with $\beta$ used as a shortcut:

$$\psi = -\frac{1}{6\xi}\left(3(\sqrt{3}C_\mathrm{I} - \xi) - \sqrt{\beta}\right),$$
$$\beta = 27C_\mathrm{I}^2 - 6\sqrt{3}C_\mathrm{I}\xi + 9\xi^2. \tag{C3}$$
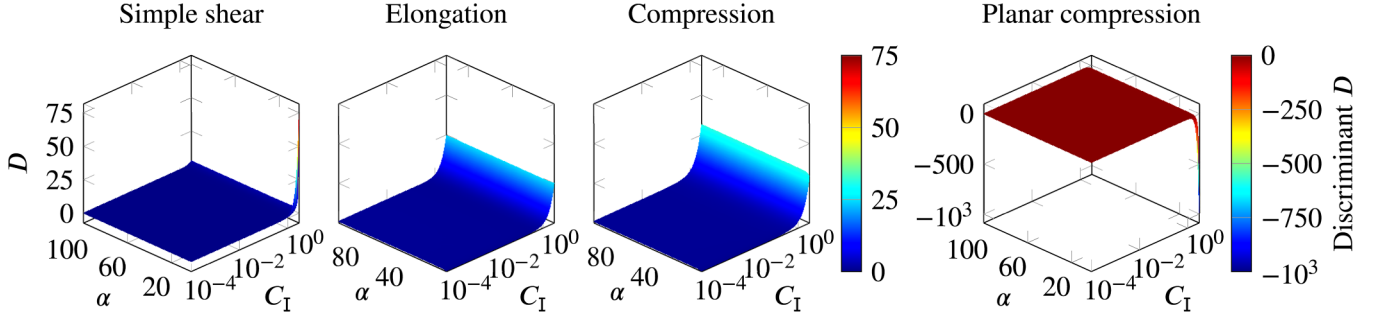
FIG. 17. Discriminant $D$ of the $\psi$-equations with respect to the fiber aspect ratio $\alpha$ and the interaction parameter $C_\mathrm{I}$ for the different investigated flow cases.

For the surface plot of $\psi$ the reader is referred to the plot of $N_{11}$ for the elongational flow in Fig. 3.

## APPENDIX D: PLANAR COMPRESSION FLOW

Analogously, the exact solution $N_{ij}$ of the following system of Eq. (D1) determines the asymptotic fiber orientation for the planar compression flow:

$$
\begin{aligned}
0 &= \xi(2N_{11} - 2(N_{11} - N_{33})N_{11}) + 2C_\mathrm{I}(1 - 3N_{11}), \\
0 &= \xi(N_{12} - 2(N_{11} - N_{33})N_{12}) - 6C_\mathrm{I}N_{12}, \\
0 &= -2\xi(N_{11} - N_{33})N_{13} - 6C_\mathrm{I}N_{13}, \\
0 &= -2\xi(N_{11} - N_{33})N_{22} + 2C_\mathrm{I}(1 - 3N_{22}), \\
0 &= \xi(-N_{23} - 2(N_{11} - N_{33})N_{23}) - 6C_\mathrm{I}N_{23}, \\
0 &= \xi(-2N_{33} - 2(N_{11} - N_{33})N_{33}) + 2C_\mathrm{I}(1 - 3N_{33}).
\end{aligned}
\tag{D1}
$$

The following equation defines $\psi$ describing the orientation state in Eq. (18):

$$
0 = 2\xi^2\psi^3 + 2\xi(3C_\mathrm{I} - \xi)\psi^2 + 3C_\mathrm{I}(C_\mathrm{I} - \xi)\psi - C_\mathrm{I}^2. \tag{D2}
$$

Based on the discriminant $D(\alpha, C_\mathrm{I}) < 0$ shown in Fig. 17 the latter equation has three real solutions for $\psi$ (see Appendix B). The physically meaningful solution $\psi$ of Eq. (D2) is as follows with $\beta$ and $\zeta$ used as a shortcut:

$$
\begin{aligned}
\psi &= \frac{1}{6\xi}\left(\beta + 6C_\mathrm{I}\sqrt{\zeta}\right)^{1/3} + \frac{9C_\mathrm{I}^2 - 3C_\mathrm{I}\xi + 2\xi^2}{3\xi\left(\beta + 6C_\mathrm{I}\sqrt{\zeta}\right)^{1/3}} - \frac{3C_\mathrm{I} - \xi}{3\xi}, \\
\beta &= 54C_\mathrm{I}^2(\xi - C_\mathrm{I}) + \xi^2(8\xi - 18C_\mathrm{I}), \\
\zeta &= -27C_\mathrm{I}^2(3C_\mathrm{I}^2 + \xi^2) - 3\xi^4.
\end{aligned}
\tag{D3}
$$

Note that the imaginary parts of $\sqrt{\zeta}$ cancel out. For the surface plot of $\psi$ the reader is referred to the plot of $N_{11}$ for the planar compression flow in Fig. 3.

## APPENDIX E: COMPRESSION FLOW

Based on the following system of Eq. (E1) written down multiplied by 2, the exact solution $N_{ij}$ for the compression flow is determined:

$$
\begin{aligned}
0 &= 2\xi(N_{11} - (N_{11} + N_{22} - 2N_{33})N_{11}) + 2\sqrt{3}C_\mathrm{I}(1 - 3N_{11}), \\
0 &= 2\xi(N_{12} - (N_{11} + N_{22} - 2N_{33})N_{12}) - 6\sqrt{3}C_\mathrm{I}N_{12}, \\
0 &= 2\xi(-N_{13}/2 - (N_{11} + N_{22} - 2N_{33})N_{13}) - 6\sqrt{3}C_\mathrm{I}N_{13}, \\
0 &= 2\xi(N_{22} - (N_{11} + N_{22} - 2N_{33})N_{22}) + 2\sqrt{3}C_\mathrm{I}(1 - 3N_{22}), \\
0 &= 2\xi(-N_{23}/2 - (N_{11} + N_{22} - 2N_{33})N_{23}) - 6\sqrt{3}C_\mathrm{I}N_{23}, \\
0 &= 2\xi(-2N_{33} - (N_{11} + N_{22} - 2N_{33})N_{33}) + 2\sqrt{3}C_\mathrm{I}(1 - 3N_{33}).
\end{aligned}
\tag{E1}
$$

By solving the following equation $\psi$ describing the orientation state in Eq. (20) is determined:

$$
0 = \xi\psi^2 - (\sqrt{3}C_\mathrm{I} + \xi)\psi + \frac{\sqrt{3}}{3}C_\mathrm{I}. \tag{E2}
$$

The latter equation results in two real solutions for $\psi$ in view of the discriminant $D(\alpha, C_\mathrm{I}) > 0$ (see Appendix B) shown in Fig. 17. The physically meaningful solution $\psi$ of Eq. (E2) is as follows with $\beta$ used as a shortcut:

$$
\begin{aligned}
\psi &= \frac{1}{6\xi}\left(3(\sqrt{3}C_\mathrm{I} + \xi) - \sqrt{\beta}\right), \\
\beta &= 27C_\mathrm{I}^2 + 6\sqrt{3}C_\mathrm{I}\xi + 9\xi^2.
\end{aligned}
\tag{E3}
$$

For the surface plot of $\psi$, the reader is referred to the plot of $N_{33}$ for the compression flow in Fig. 3.

## APPENDIX F: SIMPLE SHEAR FLOW

The asymptotic orientation state $N_{ij}$ for the simple shear flow is defined by the exact solution of following system of Eq. (F1). As stated before, the rate of deformation does not influence the asymptotic solution leading to a discontinuity in $N_{ij}$ at the centerline of infinite long channel flows,

$$
\begin{aligned}
0 &= 2N_{12} + \xi(2N_{12} - 4N_{11}N_{12}) + 2C_\mathrm{I}(1 - 3N_{11}), \\
0 &= -N_{11} + N_{22} + \xi(N_{11} + N_{22} - 4N_{12}^2) - 6C_\mathrm{I}N_{12}, \\
0 &= N_{23} + \xi(N_{23} - 4N_{12}N_{13}) - 6C_\mathrm{I}N_{13}, \\
0 &= -2N_{12} + \xi(2N_{12} - 4N_{12}N_{22}) + 2C_\mathrm{I}(1 - 3N_{22}), \\
0 &= -N_{13} + \xi(N_{13} - 4N_{12}N_{23}) - 6C_\mathrm{I}N_{23}, \\
0 &= -4\xi N_{33}N_{12} + 2C_\mathrm{I}(1 - 3N_{33}).
\end{aligned}
\tag{F1}
$$

In case of $a < 0 \, \text{s}^{-1}$, the latter system of equations can still be used but changing the sign of $N_{12}$ in Eq. (22). By solving the following equation, $\psi$ describing the orientation state in Eq. (22) is obtained:

$$0 = 4\xi^2\psi^3 + 12C_\text{l}\xi\psi^2 + (9C_\text{l}^2 - \xi^2 + 1)\psi - C_\text{l}\xi. \quad \text{(F2)}$$

Analogously, the discriminant $D(\alpha, C_\text{l}) > 0$ is shown in Fig. 17 resulting in one real and two complex solutions for $\psi$ (see Appendix B). The real solution of Eq. (F2) is as follows with $\beta$ and $\zeta$ used as a shortcut:

$$\psi = \frac{1}{6\xi}\left(\zeta + 3\sqrt{\beta}\right)^{1/3} + \frac{3C_\text{l}^2 + \xi^2 - 1}{2\xi(\zeta + 3\sqrt{\beta})^{1/3}} - \frac{C_\text{l}}{\xi},$$

$$\beta = 81C_\text{l}^4(3 - \xi^2) + 27C_\text{l}^2(2 - \xi^4 + 2\xi^2) - 3\xi^6 + 3$$
$$+ 9\xi^2(\xi^2 - 1), \quad \text{(F3)}$$

$$\zeta = 27C_\text{l}(C_\text{l}^2 + 1).$$

For the surface plot of $\psi$, the reader is referred to the plot of $N_{12}$ for the shear flow in Fig. 4.

## APPENDIX G: SUPERPOSITION—COMPRESSION AND SHEAR

The following system of Eq. (G1) (given multiplied by 2) is solved numerically for the asymptotic solution $N_{ij}$. The kinematic parameters $a, b > 0 \, \text{s}^{-1}$ only affect the asymptotic state via the ratio $a/b$. This ratio provides information about whether the shear flow or the compression flow dominates. According to Eq. (24) $a/b < 1$ represents a dominating shear and for $a/b > 1$ the compression is more distinct. The physical correct solution is found by checking for real components $N_{ij}$ first. The second step is characterized by checking the necessary properties of $N_{ij}$. Throughout this work, $N_{11} \geq 0$, $N_{22} \geq 0$ and $\text{tr}(\mathbf{N}) = 1$ is checked. This method always gives a clear result for the remaining components $N_{33}$ and $N_{12}$

$$0 = 4bN_{12} + 2\xi(aN_{11} + 2bN_{12} - (aN_{11} + aN_{22} - 2aN_{33} + 4bN_{12})N_{11}) + C_\text{l}\sqrt{12a^2 + 16b^2}(1 - 3N_{11}),$$

$$0 = -2bN_{11} + 2bN_{22} + 2\xi(bN_{11} + aN_{12} + bN_{22} - (aN_{11} + aN_{22} - 2aN_{33} + 4bN_{12})N_{12}) - 3C_\text{l}\sqrt{12a^2 + 16b^2}N_{12},$$

$$0 = 2bN_{23} + 2\xi(-aN_{13}/2 + bN_{23} - (aN_{11} + aN_{22} - 2aN_{33} + 4bN_{12})N_{13}) - 3C_\text{l}\sqrt{12a^2 + 16b^2}N_{13},$$

$$0 = -4bN_{12} + 2\xi(2bN_{12} + aN_{22} - (aN_{11} + aN_{22} - 2aN_{33} + 4bN_{12})N_{22}) + C_\text{l}\sqrt{12a^2 + 16b^2}(1 - 3N_{22}),$$

$$0 = -2bN_{13} + 2\xi(-aN_{23}/2 + bN_{13} - (aN_{11} + aN_{22} - 2aN_{33} + 4bN_{12})N_{23}) - 3C_\text{l}\sqrt{12a^2 + 16b^2}N_{23},$$

$$0 = 2\xi(-2aN_{33} - (aN_{11} + aN_{22} - 2aN_{33} + 4bN_{12})N_{33}) + C_\text{l}\sqrt{12a^2 + 16b^2}(1 - 3N_{33}).$$

(G1)

## APPENDIX H: MATERIAL PARAMETERS

In this section, the material parameters are listed for determining the anisotropic elastic behavior based on the MT method. Within this study, the glass fiber-reinforced UPPH matrix material is considered with the following values for Young's modulus $E$ and the Poisson's ratio $v$ [45]:

$$\begin{aligned} E_\text{M} &= 3.4 \, \text{GPa}, & v_\text{M} &= 0.385, \\ E_\text{F} &= 73 \, \text{GPa}, & v_\text{F} &= 0.22. \end{aligned} \quad \text{(H1)}$$

Please note that for calculating the anisotropic viscous behavior no material parameters are required besides the fiber volume fraction $\phi$ and the aspect ratio $\alpha$ within the nondimensional Dinh–Armstrong model [17]. Throughout this paper, $\phi = 0.1$ and $\alpha = 10$ are used to represent anisotropic properties.

## APPENDIX I: symQC FOR ORIENTATION EVOLUTION DESCRIPTION

First of all, it is shown that using $\mathbb{N}_{\text{symQC}}$ defined in Eq. (39) violates the condition $\text{tr}(\dot{\mathbf{N}}) = 0$. Based on $\mathbb{N}_{\text{symQC}}$,

the closure term in the FTE reads

$$\begin{aligned} \mathbb{N}_{\text{symQC}}[\mathbf{D}] &= \frac{\text{sym}(\mathbf{N} \otimes \mathbf{N})[\mathbf{D}]}{\frac{1}{3}(1 + 2\|\mathbf{N}\|^2)} \\ &= \frac{1}{\frac{1}{3}(1 + 2\|\mathbf{N}\|^2)}\frac{1}{3}\left((\mathbf{N} \cdot \mathbf{D})\mathbf{N} + 2\mathbf{NDN}\right) \\ &= \frac{1}{1 + 2\|\mathbf{N}\|^2}\left((\mathbf{N} \cdot \mathbf{D})\mathbf{N} + 2\mathbf{NDN}\right). \end{aligned} \quad \text{(I1)}$$

The condition $\text{tr}(\mathbb{N}[\mathbf{D}]) = \mathbf{D} \cdot \mathbf{N}$ given in Eq. (40) is violated by $\mathbb{N}_{\text{symQC}}$ since

$$\begin{aligned} \text{tr}(\mathbb{N}_{\text{symQC}}[\mathbf{D}]) &= \frac{1}{1 + 2\|\mathbf{N}\|^2}\left(\mathbf{N} \cdot \mathbf{D} + 2\text{tr}(\mathbf{NDN})\right) \\ &= \frac{1}{1 + 2\|\mathbf{N}\|^2}\left(\mathbf{N} \cdot \mathbf{D} + 2\mathbf{D} \cdot \mathbf{N}^2\right) \\ &\neq \mathbf{D} \cdot \mathbf{N}. \end{aligned} \quad \text{(I2)}$$

Please note that $\text{tr}(\mathbf{NDN}) = \mathbf{D} \cdot \mathbf{N}^2$ holds. The idea now is to

introduce a scalar factor $A$ in the following closure term:

$$\mathbb{N}_{\mathrm{symQC}}[\mathbf{D}] = \frac{A}{1 + 2\|\mathbf{N}\|^2}\left((\mathbf{N} \cdot \mathbf{D})\mathbf{N} + 2\mathbf{NDN}\right), \qquad \text{(I3)}$$

in such a way that the FTE is consistent in the sense of the trace conservation of $\mathbf{N}$,

$$\frac{A}{1 + 2\|\mathbf{N}\|^2}\left(\mathbf{N} \cdot \mathbf{D} + 2\mathbf{D} \cdot \mathbf{N}^2\right) \overset{!}{=} \mathbf{D} \cdot \mathbf{N}. \qquad \text{(I4)}$$

After a quick analysis, the process-dependent quantity $A$ can be eliminated

$$A = \frac{(1 + 2\|\mathbf{N}\|^2)\,\mathbf{N} \cdot \mathbf{D}}{\mathbf{N} \cdot \mathbf{D} + 2\mathbf{D} \cdot \mathbf{N}^2}. \qquad \text{(I5)}$$

By inserting Eq. (I5) into Eq. (I3), the sought closure function being nonlinear in $\mathbf{D}$ is as follows:

$$\begin{aligned}\mathbb{N}_{\mathrm{symQC}}[\mathbf{D}] &= \frac{\mathbf{N} \cdot \mathbf{D}}{\mathbf{N} \cdot \mathbf{D} + 2\mathbf{D} \cdot \mathbf{N}^2}\left((\mathbf{N} \cdot \mathbf{D})\mathbf{N} + 2\mathbf{NDN}\right) \\ &= \frac{3\,\mathbf{N} \cdot \mathbf{D}}{\mathbf{N} \cdot \mathbf{D} + 2\mathbf{D} \cdot \mathbf{N}^2}\,\mathrm{sym}(\mathbf{N} \otimes \mathbf{N})[\mathbf{D}] \\ &= \mathbf{G}(\mathbf{N}, \mathbf{D}).\end{aligned} \qquad \text{(I6)}$$

It should be noted that the term $1 + 2\|\mathbf{N}\|^2$ introduced in Eq. (39) cancels out. Furthermore, $\mathbf{G}$ is a homogeneous function of degree 1 in $\mathbf{D}$. The definition of $\kappa$ given in Eq. (42) and applied in Eq. (43) is based on considering the complete closure term of the FTE

$$2\mathbb{N}[\mathbf{D}] \approx \kappa\,\mathrm{sym}(\mathbf{N} \otimes \mathbf{N})[\mathbf{D}], \quad \kappa = \frac{6\,\mathbf{N} \cdot \mathbf{D}}{\mathbf{N} \cdot \mathbf{D} + 2\mathbf{D} \cdot \mathbf{N}^2}. \qquad \text{(I7)}$$

By looking at Eq. (I7), the isotropic fiber orientation state $\mathbf{N}_{\mathrm{ISO}} = \mathbf{I}/3$ is critical in view of incompressible flows since $\mathrm{tr}(\mathbf{D}) = \mathbf{D} \cdot \mathbf{I} = 0$ causes a division by zero. For this case, $\kappa = 0$ is sufficient resulting in the same strain rate part of the FTE as for the QC preserving $\mathrm{tr}(\mathbf{N}) = 1$. In addition, for flows with vanishing strain rate $\mathbf{D} = \mathbf{0}$, the direction of the strain rate is not defined and $\kappa = 0$ also applies. During the simulations, nontrivial singularities of the form $\mathbf{D} \cdot \mathbf{N} \neq 0$ and $\mathbf{D} \cdot \mathbf{N} + 2\mathbf{D} \cdot \mathbf{N}^2 = 0$ must be excluded $\forall \mathbf{D} \neq \mathbf{0}, \mathbf{N} \neq \mathbf{N}_{\mathrm{iso}}$. This is part of further research. These singularities exist, as the following example shows

$$D_{ij} = \begin{pmatrix} 1 & 0 & 0 \\ 0 & 1 & 0 \\ 0 & 0 & -2 \end{pmatrix}, \quad N_{ij} = \begin{pmatrix} \frac{51-7\sqrt{33}}{20} & 0 & 0 \\ 0 & \frac{1}{10} & 0 \\ 0 & 0 & \frac{-33+7\sqrt{33}}{20} \end{pmatrix},$$

$$\mathbf{D} \cdot \mathbf{N} = \frac{119 - 21\sqrt{33}}{20}, \quad 0 = \mathbf{D} \cdot \mathbf{N} + 2\mathbf{D} \cdot \mathbf{N}^2. \qquad \text{(I8)}$$

Any nonsingular states $0 \approx \mathbf{D} \cdot \mathbf{N} + 2\mathbf{D} \cdot \mathbf{N}^2$ and $\mathbf{D} \cdot \mathbf{N} \neq 0$ have to be treated numerically by small time steps to sufficiently resolve $\dot{\mathbf{N}}$. Correction schemes used in other studies [10,60,61] may apply to ensure the necessary algebraic

properties of the solution $\mathbf{N}$. The special case of 2D fiber orientation states and incompressible suspensions,

$$N_{ij} = \begin{pmatrix} N_{11} & N_{12} \\ N_{12} & 1 - N_{11} \end{pmatrix}, \quad D_{ij} = \begin{pmatrix} D_{11} & D_{12} \\ D_{12} & -D_{11} \end{pmatrix}, \qquad \text{(I9)}$$

leads to $\kappa = 2$ since $\mathbf{D} \cdot \mathbf{N} = \mathbf{D} \cdot \mathbf{N}^2$. Please note that for this case $\mathbf{D} \neq \mathbf{0}$ and $\mathbf{N} \neq \mathbf{N}_{\mathrm{iso}}$ is required in 2D. Otherwise, $\kappa = 0$ holds for $\mathbf{D} = \mathbf{0}$ or $\mathbf{N} = \mathbf{N}_{\mathrm{iso}}$ as already described.

## NOMENCLATURE

| | |
|---|---|
| $A$ | Correction factor symQC (—) |
| $a, b$ | Deformation rates (s$^{-1}$) |
| $a_m^n, c_m^n$ | Coefficients orientation tensors (—) |
| $\mathbf{B}_t$ | Base tensors (—) |
| $\mathbb{B}_{t\gamma}$ | Base tensors (—) |
| $b_i$ | Coefficients orientation average (Pa) |
| $C_{\mathrm{I}}$ | Fiber-fiber interaction parameter (—) |
| $\mathbb{C}$ | Stiffness tensor (Pa) |
| $D$ | Discriminant of $\psi$-equation (—) |
| $D_i$ | Eigenvalues of $\mathbf{D}_0$ (s$^{-1}$) |
| $\mathbf{D}, \mathbf{D}_0$ | Strain rate tensors (s$^{-1}$) |
| $\mathbf{d}$ | Tensile/shear direction (—) |
| $E$ | Young's modulus (Pa) |
| $e$ | Closure error (—) |
| $\mathbf{e}_i$ | Cartesian base vectors (—) |
| $\mathbf{e}_i^{\mathsf{H}}$ | Eigenvectors of $\mathbf{D}_0$ (—) |
| $\mathbb{F}$ | Closure function (—) |
| $f$ | Probability density function (—) |
| $\mathbf{G}$ | Closure function (s$^{-1}$) |
| $\mathbf{I}$ | Identity on first-order tensors (—) |
| $\mathbb{I}$ | Identity on second-order tensors (—) |
| $\mathbb{I}^{\mathsf{S}}$ | Identity on sym. sec.-order tensors (—) |
| $\mathbb{K}$ | Kinematics tensor (s$^{-1}$) |
| $k_i, \tilde{k}_i, p, q$ | Abbreviations within $D$ (—) |
| $\mathscr{L}$ | Argument list of $\mathbf{R}$ (—) |
| $\mathbf{L}$ | Velocity gradient (s$^{-1}$) |
| $N_{\mathrm{cells}}$ | Number of grid cells (—) |
| $\mathbf{N}$ | First-kind orientation tensor (—) |
| $\mathbb{N}$ | First-kind orientation tensor (—) |
| $\mathbb{N}_{\langle n \rangle}^{(k)}$ | n*th*-order, k*th*-kind orientation tensor (—) |
| $n$ | Tensor order (even) (—) |
| $\mathbf{n}$ | Fiber direction (—) |
| $\mathbb{P}_0$ | Polarization tensor (Pa$^{-1}$) |
| $\mathbb{P}_1, \mathbb{P}_2$ | Projectors (—) |
| $\mathbf{p}$ | Shear plane normal (—) |
| $\mathbf{Q}, \mathbf{Q}_{\mathsf{D}}$ | Orthogonal tensors (—) |
| $\mathbf{R}$ | Right-hand side of FTE (s$^{-1}$) |
| $\mathscr{S}$ | Surface of unit sphere (—) |
| $\mathbb{T}$ | Abbreviation within Mori–Tanaka (Pa) |
| $t$ | Time (s) |
| $V, V_i$ | Domain/cell volume (m$^3$) |
| $\mathbb{V}$ | Viscosity tensor (Pa s) |
| $\mathbf{W}$ | Spin tensor (s$^{-1}$) |
| $\mathbf{x}$ | Actual placement (m) |

### Greek

| | |
|---|---|
| $\alpha$ | Fiber aspect ratio (—) |

| | |
|---|---|
| $\dot{\gamma}$ | Shear rate ($s^{-1}$) |
| $\eta, \eta_M, \eta_1$ | Shear viscosities (Pa s) |
| $\kappa$ | Correction factor symQC (—) |
| $\Lambda$ | Parameter spin-free flows (—) |
| $\nu$ | Poisson's ratio (—) |
| $\xi$ | Fiber shape parameter (—) |
| $\phi$ | Fiber volume fraction (—) |
| $\varphi, \theta$ | Angles spherical coordinates (rad) |
| $\psi, \beta, \zeta$ | Abbreviations asymptotic states (—) |

## Abbreviation

| | |
|---|---|
| 2D/3D | Two-/three-dimensional |
| BFS | Backward-facing step flow |
| CF | Channel flow |
| F | Fiber |
| FTE | Folgar–Tucker equation |
| IBOF | Invariant-based optimal fitting |
| ISO | Isotropic |
| M | Matrix |
| MT | Mori–Tanaka method |
| OA | Orientation average |
| PDF | Probability density function |
| PI | Planar isotropic |
| QC | Quadratic closure |
| symQC | Symmetric quadratic closure |
| UD | Unidirectional |

## REFERENCES

[1] Ashby, M. F., *Materials Selection in Mechanical Design* (Springer, Berlin, 2006).

[2] Henning, F., and E. Moeller, *Handbuch Leichtbau* (Hanser, München, 2011).

[3] Karl, T., D. Gatti, T. Böhlke, and B. Frohnapfel, "Coupled simulation of flow-induced viscous and elastic anisotropy of short-fiber reinforced composites," Acta Mech. **232**, 2249–2268 (2021).

[4] Advani, S. G., and C. L. Tucker, "The use of tensors to describe and predict fiber orientation in short fiber composites," J. Rheol. **31**, 751–784 (1987).

[5] Kanatani, K.-I., "Distribution of directional data and fabric tensors," Int. J. Eng. Sci. **22**, 149–164 (1984).

[6] Advani, S. G., and C. L. Tucker, "Closure approximations for three-dimensional structure tensors," J. Rheol. **34**, 367–386 (1990).

[7] Chung, D. H., and T. H. Kwon, "Improved model of orthotropic closure approximation for flow induced fiber orientation," Polym. Compos. **22**, 636–649 (2001).

[8] Chung, D. H., and T. H. Kwon, "Invariant-based optimal fitting closure approximation for the numerical prediction of flow-induced fiber orientation," J. Rheol. **46**, 169–194 (2002).

[9] Cintra, J. S., and C. L. Tucker, "Orthotropic closure approximations for flow-induced fiber orientation," J. Rheol. **39**, 1095–1122 (1995).

[10] Kuzmin, D., "Planar and orthotropic closures for orientation tensors in fiber suspension flow models," SIAM J. Appl. Math. **78**, 3040–3059 (2018).

[11] Montgomery-Smith, S., W. He, D. A. Jack, and D. E. Smith, "Exact tensor closures for the three-dimensional Jeffery's equation," J. Fluid Mech. **680**, 321–335 (2011).

[12] Montgomery-Smith, S., D. Jack, and D. E. Smith, "The fast exact closure for Jeffery's equation with diffusion," J. Non-Newtonian Fluid Mech. **166**, 343–353 (2011).

[13] Folgar, F., and C. L. Tucker, "Orientation behavior of fibers in concentrated suspensions," J. Reinf. Plast. Compos. **3**, 98–119 (1984).

[14] Altan, M. C., and L. Tang, "Orientation tensors in simple flows of dilute suspensions of non-Brownian rigid ellipsoids, comparison of analytical and approximate solutions," Rheol. Acta **32**, 227–244 (1993).

[15] Bretherton, F. P., "The motion of rigid particles in a shear flow at low Reynolds number," J. Fluid Mech. **14**, 284–304 (1962).

[16] Doi, M., "Molecular dynamics and rheological properties of concentrated solutions of rodlike polymers in isotropic and liquid crystalline phases," J. Polym. Sci., Polym. Phys. Ed. **19**, 229–243 (1981).

[17] Dinh, S. M., and R. C. Armstrong, "A rheological equation of state for semi-concentrated fiber suspensions," J. Rheol. **28**, 207–227 (1984).

[18] Mori, T., and K. Tanaka, "Average stress in matrix and average elastic energy of materials with misfitting inclusions," Acta Metall. **21**, 571–574 (1973).

[19] Jeffery, G. B., and L. N. G. Filon, "The motion of ellipsoidal particles immersed in a viscous fluid," Proc. R. Soc. London, Ser. A **102**, 161–179 (1922).

[20] Mönnich, S., Entwicklung einer Methodik zur Parameteridentifikation für Orientierungsmodelle in Spritzgießsimulationen, Doctoral thesis, Otto-von-Guericke-Universität, Magdeburg, 2015.

[21] Petrie, C. J., "The rheology of fibre suspensions," J. Non-Newtonian Fluid Mech. **87**, 369–402 (1999).

[22] Verleye, V., and F. Dupret, Prediction of fiber orientation in complex injection molded parts, *Developments in Non-Newtonian Flows* (American Society of Mechanical Engineers, New York, 1993), Vol. 175, pp. 139–164.

[23] Altan, M. C., S. I. Güceri, and R. Pipes, "Anisotropic channel flow of fiber suspensions," J. Non-Newtonian Fluid Mech. **42**, 65–83 (1992).

[24] Okagawa, A., R. Cox, and S. Mason, "The kinetics of flowing dispersions. VI. Transient orientation and rheological phenomena of rods and discs in shear flow," J. Colloid Interface Sci. **45**, 303–329 (1973).

[25] Moosaie, A., Direct numerical simulation of turbulent drag reduction by rigid fiber additives, Doctoral thesis, Technische Universität München, 2011.

[26] Carlson, B., "Numerical computation of real or complex elliptic integrals," Numer. Algorithms **10**, 13–26 (1995).

[27] Carlson, B., and E. M. Notis, "Algorithm 577—Algorithms for incomplete elliptic integrals [S21]," ACM Trans. Math. Softw. **7**, 398–403 (1981).

[28] Gurtin, M. E., E. Fried, and L. Anand, *The Mechanics and Thermodynamics of Continua* (Cambridge University, New York, 2010).

[29] Ospald, F., Contributions to the simulation and optimization of the manufacturing process and the mechanical properties of short fiber-reinforced plastic parts, Doctoral thesis, Technische Universität Chemnitz, 2019.

[30] Latz, A., U. Strautins, and D. Niedziela, "Comparative numerical study of two concentrated fiber suspension models," J. Non-Newtonian Fluid Mech. **165**, 764–781 (2010).

[31] Böhlke, T., and A. Bertram, "Asymptotic values of elastic anisotropy in polycrystalline copper for uniaxial tension and compression," Comput. Mater. Sci. **26**, 13–19 (2003).

[32] Moakher, M., "Fourth-order cartesian tensors: Old and new facts, notions and applications," Q. J. Mech. Appl. Mech. **61**, 181–203 (2008).

[33] Moakher, M., and P. J. Basser, Fiber orientation distribution functions and orientation tensors for different material symmetries, in *Visualization and Processing of Higher Order Descriptors for Multi-Valued Data*, edited by I. Hotz and T. Schultz (Springer International, Berlin, 2015), pp. 37–71.

[34] Schemmann, M., Biaxial Characterization and Mean-field Based Damage Modeling of Sheet Molding Compound Composites, Doctoral

thesis, Schriftenreihe Kontinuumsmechanik im Maschinenbau Band 13, Karlsruher Institut für Technologie (KIT), 2018.

[35] Mezi, D., G. Ausias, S. G. Advani, and J. Férec, "Fiber suspension in 2D nonhomogeneous flow: The effects of flow/fiber coupling for Newtonian and power-law suspending fluids," J. Rheol. **63**, 405–418 (2019).

[36] Bertóti, R., and T. Böhlke, "Flow-induced anisotropic viscosity in short FRPs," Mech. Adv. Mater. Modern Processes **3**, 1 (2017).

[37] Bay, R. S., Fiber orientation in injection molded composites: A comparison of theory and experiment, Doctoral thesis, University of Illinois at Urbana-Champaign, 1991.

[38] Phan-Thien, N., X.-J. Fan, R. Tanner, and R. Zheng, "Folgar-Tucker constant for a fibre suspension in a Newtonian fluid," J. Non-Newtonian Fluid Mech. **103**, 251–260 (2002).

[39] Wang, J., J. F. O'Gara, and C. L. Tucker, "An objective model for slow orientation kinetics in concentrated fiber suspensions: Theory and rheological evidence," J. Rheol. **52**, 1179–1200 (2008).

[40] Kugler, S., A. Kech, C. Cruz, and T. Osswald, "Fiber orientation predictions—A review of existing models," J. Compos. Sci. **4**, 69 (2020).

[41] Böhlke, T., Crystallographic texture evolution and elastic anisotropy—Simulation, modeling, and applications, Doctoral thesis, Otto-von-Guericke-Universität Magdeburg, 2001.

[42] Torquato, S., *Random Heterogeneous Materials: Microstructure and Macroscopic Properties* (Springer, New York, 2002).

[43] Brylka, B., Charakterisierung und Modellierung der Steifigkeit von langfaserverstärktem Polypropylen, Doctoral thesis, Schriftenreihe Kontinuumsmechanik im Maschinenbau Band 10, Karlsruher Institut für Technologie (KIT), 2017.

[44] Tucker, C. L., "Flow regimes for fiber suspensions in narrow gaps," J. Non-Newtonian Fluid Mech. **39**, 239–268 (1991).

[45] Kehrer, L., J. T. Wood, and T. Böhlke, "Mean-field homogenization of thermoelastic material properties of a long fiber-reinforced thermoset and experimental investigation," J. Compos. Mater. **54**, 3777–3799 (2020).

[46] Böhlke, T., and C. Brüggemann, "Graphical representation of the generalized Hooke's law," Tech. Mech. **21**, 145–158 (2001); available at https://journals.ub.ovgu.de/index.php/techmech/article/view/1045.

[47] Voigt, W., *Lehrbuch der Kristallphysik* (Teubner, Leipzig, 1910).

[48] Férec, J., D. Mezi, S. G. Advani, and G. Ausias, "Axisymmetric flow simulations of fiber suspensions as described by 3D probability distribution function," J. Non-Newtonian Fluid Mech. **284**, 104367 (2020).

[49] Dupret, F., and V. Verleye, "Modelling the flow of fiber suspensions in narrow gaps," Rheol. Ser. **8**, 1347–1398 (1999).

[50] Mattheck, C., *Thinking Tools After Nature* [Karlsruhe Institute of Technology (KIT), Campus North, Karlsruhe, 2011].

[51] Schmidt, M.-P., L. Couret, C. Gout, and C. B. W. Pedersen, "Structural topology optimization with smoothly varying fiber orientations," Struct. Multidiscipl. Optim. **62**, 3105–3126 (2020).

[52] Petty, C. A., S. M. Parks, and S. M. Shao, Flow-induced alignment of fibers, in *Proceedings of 12th International Conference on Composite Materials ICCM-12, Paris* (Torres, Paris, 1999).

[53] Hinch, E. J., and L. G. Leal, "Constitutive equations in suspension mechanics. Part 2. Approximate forms for a suspension of rigid particles affected by Brownian rotations," J. Fluid Mech. **76**, 187–208 (1976).

[54] Deuflhard, P., and F. Bornemann, *Numerische Mathematik 2—Gewöhnliche Differentialgleichungen* (De Gruyter, Berlin, 2008).

[55] Kalidindi, S. R., J. R. Houskamp, M. Lyons, and B. L. Adams, "Microstructure sensitive design of an orthotropic plate subjected to tensile load," Int. J. Plast. **20**, 1561–1575 (2004).

[56] Shaffer, J. B., M. Knezevic, and S. R. Kalidindi, "Building texture evolution networks for deformation processing of polycrystalline fcc metals using spectral approaches: Applications to process design for targeted performance," Int. J. Plast. **26**, 1183–1194 (2010).

[57] Ehrentraut, H., and W. Muschik, "On symmetric irreducible tensors in d dimensions: Introduction and motivation," ARI - Int. J. Phys. Eng. Sci. **51**, 149–159 (1998).

[58] Arens, T., F. Hettlich, C. Karpfinger, U. Kockelkorn, K. Lichtenegger, and H. Stachel, *Mathematik* (Springer, Berlin, 2018).

[59] Merziger, G., G. Mühlbach, D. Wille, and T. Wirth, *Formeln + Hilfen Höhere Mathematik* (Binomi, Barsinghausen, 2018).

[60] Paschkewitz, J. S., Y. Dubief, C. D. Dimitropoulos, E. S. G. Shaqfeh, and P. Moin, "Numerical simulation of turbulent drag reduction using rigid fibres," J. Fluid Mech. **518**, 281–317 (2004).

[61] Verweyst, B. E., and C. L. Tucker, "Fiber suspensions in complex geometries: Flow/orientation coupling," Can. J. Chem. Eng. **80**, 1093–1106 (2002).